Matrix Isolation Infrared and ab-initio study of Hydrogen Bonded Complexes Between Phenylacetylene and Chloroform

Deepak Verma

A dissertation submitted for the partial fulfilment of BS-MS dual degree in Science

Indian Institute of Science Education and Research Mohali
April 2014

Certificate of Examination

This is to certify that the dissertation titled "Matrix Isolation Infrared and ab-initio Study of Hydrogen Bonded Complexes Between Phenylacetylene-D and Chloroform" submitted by Mr. Deepak Verma (Reg. No. MS09046) for the partial fulfilment of BS-MS dual degree programme of the Institute, has been examined by the thesis committee duly appointed by the Institute. The committee finds the work done by the candidate satisfactory and recommends that the report be accepted.

Dr. Sugumar Venkataramani Dr. P.Balanarayan Prof. K.S. Viswanathan (Supervisor)

Dated: April 25, 2014

Declaration

The work presented in this dissertation has been carried out by me under the guidance of Prof. K. S Viswanathan at the Indian Institute of Science Education and Research Mohali.

This work has not been submitted in part or in full for a degree, a diploma, or a fellowship to any other university or institute. Whenever contributions of others are involved, every effort is made to indicate this clearly, with due acknowledgement of collaborative research and discussions. This thesis is a bonafide record of original work done by me and all sources listed within have been detailed in the bibliography.

Deepak Verma
(Candidate)
Dated: 25, April 2014

In my capacity as the supervisor of the candidate's project work, I certify above statements by the candidate are true to the best of my knowledge

Prof. K.S. Viswanathan
(Supervisor)

Acknowledgment

I would like to express my sincere gratitude to my master dissertation supervisor Prof. K.S Viswanathan, Head of the Department of Chemical Sciences, IISER Mohali. I heartily value his advice, expert guidance, valuable suggestions, discussions and constant encouragement imparted during the course of this work and preparation of the thesis. He is one among the few reasons which made me think that I should pursue a career in science and I am grateful to him. I had a great work experience under his guidance.

I am also grateful to my Master's thesis committee members Dr. Sugumar Venkataramani and Dr. P.Balanarayan for their valuable suggestions and comments during the committee meeting.

I am grateful to my lab members Kanupriya Verma, Ginny Karir, Jyoti Saini and Mariyam Fatima who accompanied me throughout this research work. I owe special thanks to Dr. Bishnu Prasad Kar, Gaurav Kumar and Kapil Dave for familiarising us with the experimental and computational techniques during the initial stages of work.

I thank each one of my classmates who provided a wonderful and friendly atmosphere to carry out research during the entire period. It is my pleasure to thank each and every member of the Department of Chemical Sciences who have helped me in various ways during the course of investigation and research. In addition, I express my gratitude to the non-academic staff of IISER Mohali for helping us out in each and every single aspect of my experimental research.

I wish to acknowledge the Computing Facility staff for providing me excellent facilities during the computational work. I am extremely thankful to Prof. N. Sathyamurthy, Director, IISER Mohali, for allowing me to use the various facilities of this institute to carry out the research work.

I would also like to acknowledge the "Department of Science and Technology, India" and "Indian Institute of Science" for providing the KVPY Scholarship.

Last but not the least, I express my sincere gratitude to each of my family members for their encouragement and moral support throughout the course of study.

List of Figures

List of Tables

List of Notations

PhAc-D	Phenylacetylene-D
$CHCl_3$	Chloroform
$CDCl_3$	Chloroform-D
FT	Fourier Transform
Ac	Acetylene
UV	Ultravoilet
Elec	Electrostatic
Ind	Inductive
Dis	Dispersive
Rep	Repulsive
GM	Grifford-McMahon
KBr	Potassium Bromide
HF	Hartree-Fock
DFT	Density Functional Theorem
CI	Configuration interaction
CC	Coupled Cluster
MRCI	Multi-reference configuration interaction
B3LYP	Becke-3-Lee-Yang-Parr
M06	Minnesota functional
FWHM	Full width at half maximum
ZPE	Zero Point Energy
BSSE	Basis Set Superposition Error
AIM	Atoms in Molecules

Contents

Abstract

Non covalent and weak interactions form an important part of various chemical and biological systems among which hydrogen bonding plays the most important role. Over the last few decades, this interaction has been widely studied and well appreciated. Only recently, weak hydrogen bonding such as O-H… π and C-H… π has drawn considerable attention.

Several spectroscopic techniques have been employed for the studies of such hydrogen bonded interaction in molecules including IR and NMR studies. One such technique is matrix isolation infrared spectroscopy, which serves as a powerful tool for exploring weak interactions and conformations. This technique has several advantages such sharp spectral features, absence of collisional and Doppler broadening and populating in only a few rovibronic levels.

The current study involves the study of weak non-covalent interactions between two molecules of interest namely, phenylacetylene and chloroform both computationally and experimentally. The experimental technique utilized for the study is matrix isolation IR while GAUSSIAN 09 software is employed for the computations. The motivation behind choosing these two molecules is that they possess multiple hydrogen bonding sites and therefore it becomes interesting to investigate the hierarchy of hydrogen bonding in such systems.

The main aim of this study is to elucidate the structures of the various hydrogen bonded complexes between the two precursor molecules. The computational work has been performed at B3LYP and M06-2X level of theory using 6-311++G(d,p) basis set. The calculations reveal the formation of four different complexes between the two monomers. The most dominating interaction observed computationally is the C-H… π which is confirmed by the experiments through the shifts observed in the vibrational frequencies of the submolecules in the complexes.

CHAPTER 1

Introduction

All matter is held together by force. The force between atoms within a molecular is a chemical or intramolecular force. The force between molecules is a physical or intermolecular force. The intermolecular forces are weaker than intramolecular forces (the chemical bonds within an individual molecule). This distinction is the reason we define the molecule in the first place.

Non covalent forces were first recognized by the Dutch scientist Johannes Diderik van der Waals. A non-covalent interaction differs from a covalent bond in that it does not involve the sharing of electrons, but rather involves more dispersed variation of interactions between molecules or within a molecule [1]. The energy released in the formation of non-covalent interactions is typically on the order of 1-5 kcal/mol [2]. The various non-covalent interaction can be classified as:

- **Electrostatic interaction**: Electrostatic interaction result from a complete transfer of electrons from one atom to another, resulting in two ions of opposite charge. The ionic character between the atoms is mainly due to the electronegativity difference, causing the bonding to be more polar than in covalent bonding where electrons are shared more equally. Ionic bonds are often 250-4000 kcal/mol in strength [3].
- **Van der Waals interactions**: Van der Waals interaction is the sum of attractive or repulsive forces between molecules that result from correlations in the fluctuating polarizations of nearby particles [4]. Such forces are relatively weak compared to covalent bonds but are fundamental to various chemical processes. The commonly known attractive intermolecular forces are dipole-dipole, induced dipole-dipole and London dispersion forces.

- **Hydrogen Bonds**: A hydrogen bond is a type of attractive (dipole-dipole) interaction between an electronegative atom (N,O,F) and a hydrogen atom bonded to another electronegative atom. A hydrogen bond tends to be stronger than van der Waals interaction, but weaker than covalent and ionic bonds. Typical strength of hydrogen bond ranges from 1-12 kcal/mol.

- **Hydrophobic interactions**: The hydrophobic effect is the tendency of nonpolar substances to aggregate in aqueous solution and exclude water molecules [5]. The hydrophobic interaction is mostly an entropy driven process and thus intrinsically temperature sensitive. It is considered to be the major driving force for the folding of globular proteins. Hydrophobic interactions are relatively stronger than other weak intermolecular forces (i.e van der Waals forces)

Pi effect:

π interactions are a type of electrostatic interactions where a region of negative charge interacts with a positive charge, the electron rich pi system can interact with a cation, an anion, another molecule and even another pi system[6]. Cation pi interaction is an example of non covalent bonding between a monopole (cation) and a quadrapole (pi system). CH-pi interactions are similar type of interaction of C-H with pi system. These interactions are caused largely from dispersion and partly from charge transfer and electrostatic forces. The strength of CH-pi interactions ranges from 1.5-2.5 Kcal/mol.

1.1 HYDROGEN BOND

Hydrogen bonding is an extensively studied interaction which has significant implications in chemical and biological processes. Its functional importance stems from both thermodynamics and kinetic reasons [7].

Based on earlier definitions, hydrogen bonding interactions exist between molecules containing an electronegative atom possessing lone pairs of electrons (Usually O, N, or F), called acceptors (A) and molecules containing covalent bonds between hydrogen and an electronegative atom (Usually O-H, N-H, S-H), called donors (D). The polarized nature of the X-H bond (X=O,N,…) results in a highly electropositive hydrogen which is attracted towards bond formation with the electron rich electronegative acceptor atoms.

The preferred geometry of the hydrogen bond is a linear conformation, with the hydrogen atom positioned along the line connecting the heteroatoms. This preferred geometry, however is not always obtained in nature due to the constraints of the neighbouring covalent systems, which are much less easily distorted. This property of the hydrogen bond leads to its directionality. The strength of individual hydrogen bonds range from 1-10 Kcal/mol which leads to longer, weaker bonds compared to covalent bonds (70-110 Kcal/mol)[8].

1.1.1 History and definition:

Between the beginning of the twentieth century and the late 1930's many descriptions of interactions between hydrogen atoms in molecules and electronegative atoms to which these hydrogens were bound non covalently appeared [9].

In 1920, Latimer and Rodebush, working on the structure and properties of water with G.N Lewis at UC Berkeley proposed,

" *A free pair of electrons on one water molecule might be able to exert sufficient force on a hydrogen held by a pair of electrons on another water molecule to bind the two molecules together…such an explanation amounts to saying that the hydrogen nucleus held between 2 octet constitutes a weak 'bond'* [10]"

This Lewis dot formalism, was the first to truly call this interaction a bond. This phenomenon really reached acceptance in the main stream only through Pauling's paper in 1939 on 'the nature of the chemical bond [11]' and its seminal chapter "the hydrogen bond". It read,

" *Under certain conditions an atom of hydrogen is attracted by rather strong forces to two atoms, instead of only one, so that it may be considered to be acting as a bond between them. This is called the hydrogen bond*"

Pauling's description of hydrogen bond on quantum mechanical grounds were,

" *A hydrogen atom, with only one stable orbital, cannot form more than one pure covalent bond and that the attraction of two atoms observed in hydrogen-bond formation must be due largely to ionic forces*"

A much broader, operational definition was provided by Pimental and McClellan in their 1960 book, "The Hydrogen Bond [12]

" A H-bond exists between a functional group A-H and an atom or a group of atoms B in the same or a different molecule when (a) there is an evidence of bond formation (association or chelation) (b) there is evidence that this new bond linking A-H and B specifically involves the hydrogen atom already bonded to A"

Both experiment and theory have shown, this is indeed a more corrected definition. This rather broad definition leaves open the possibility of hydrogen bonding to groups of atoms which are not themselves highly electronegative, or the involvement of hydrogen atoms covalently bond to non-electronegative atoms such as carbon.

In a symposium held in 1957, Coulson in his paper titled "the hydrogen bond" presented a review of the status of theory in its attempts to understand and explain hydrogen bonding. Coulson discounted the electrostatic model of hydrogen bonding, which owed much to the work of Lennard-Jones and Pople [13] as insufficient to account for all the phenomenon associated with hydrogen bonding. Instead, Coulson divided the Columbic attraction energy of hydrogen bond into four causative factors: electrostatic, covalent, repulsive and dispersion contributions. Almost 20 years later, Kitaura and Morokuma, through a scheme within the framework of ab-initio SCF theory (NEDA) suggested that hydrogen bonds between neutral donors and acceptors were "*strongly electrostatic in nature, with a small but significant contribution of charge transfer* [14]". Furthermore, the uniqueness of hydrogen bonding was simply and unassumingly that "*it always involves a moderately polar, short and strong [H-A] bond as the proton donor* [14] ".

Over the years, the definition of hydrogen bond has kept changing from author to author. After remaining ambiguous for a long time, the exact definition (and modern) of a true hydrogen bond was revealed by a task group formed by IUPAC, consisting of 25 experts from all over the world [15].

"The hydrogen bond is an attractive interaction between a hydrogen atom from a molecule or a molecular fragment X–H in which X is more electronegative than H, and an atom or a group of atoms in the same or a different molecule, in which there is evidence of bond formation".

According to the conventional definition, Hydrogen bond is a noncovalent, attractive interaction between a proton donor X-H and a proton acceptor Y in the same or in different molecule.

X-H…..Y

The H atom is bonded to electronegative atoms such as N,O and F. Y is either an electronegative region or a region of electron excess[16]. However experimental and theoretical results reveal that even C-H can be involved in H-bonds and pi electrons can act as proton acceptors in the stabilization of weak H-bonding interactions in many chemical systems [17,18].

In classical H-bonding, there is a shortening of X…Y distance, if X-H is H-bonded to Y. The distance between X….Y is less than the sum of the Van Der Waal radii of the two atoms X and Y. H-bonding interaction leads to increase in the X-H bond distance. As a consequence, a substantial red shift (of the order of 100 cm-1) is observed in the fundamental X-H stretching frequencies [19].

1.2 Properties:

1.2.1 Bond Energy:

Various spectroscopic techniques have been employed for the investigation of hydrogen bonds and their strengths. Hydrogen bonds have been classified into three types based on their bond energies: Weak, Moderate and Strong. The strength of these bonds is determined by two main factors. The first one is the charges on the donor and the acceptor groups which increase the electron density of the acceptor groups or deshield the proton. The second one is a constraint on the configuration space that forces a close contact between the donor and acceptor. **Table 1** summarizes other differences between the three types of H-Bonds.

1.2.2 Vibrational properties:

As an H-bond is formed, there is a restriction in the degree of vibrational motion since the hydrogen atom in the X-H bond is restrained by two bonds rather than one. As a consequence of the weakening of the X-H bond, the X-H stretching vibration is generally observed to shift to a lower frequency. The shift in X-H frequency upon complexation is denoted as $\Delta\nu_s = \nu_s(XH\ldots Y) - \nu(X\text{-}H)$

H Bond parameters	**Strong**	**Moderate**	**Weak**
Interaction type	Strongly covalent	Mostly electrostatic	Electrostatic/dispersed
Bond lengths (H…Y[Å])	1.2-1.5	1.5-2.2	>2.2
Lengthening of X-H (Å)	0.08-0.25	0.02-0.08	<0.02
X-H Vs H…Y	X-H ≈ H…Y	X-H < H…Y	X-H << H…Y
H bond length(X.Y [Å])	2.2-2.5	2.5-3.2	>3.2
Directionality	Strong	Moderate	Weak
H-bond angles (°)	170-180	>130	>90
H-bond strength (Kcal/mol)	15-40	4-15	<4
Relative infrared shift (cm-1)	25%	10-25%	<10%

Table 1 : Types of Hydrogen bonds and some of their properties

This shift in the vibrational frequency is often used as the simplest criterion for spectroscopic analysis and a proof for the existence of hydrogen bonding.

1.2.3 Potential Energy surfaces:

Potential energy surfaces are significantly affected (and modified) depending upon the strength of hydrogen bond. Typically, in a hydrogen bonding situation, the potential energy curves become broader and there is a possibility of a second minimum to develop. As a consequence, the X-H bond stretching vibrational levels become closer. **Fig 1** below shows several possible potential energy curves for an O-H…O hydrogen bond [69].

Fig (a) shows an asymmetric double well potential, where the hydrogen is attached more strongly to one oxygen than the other. This type of situation arises when the acceptor atoms are not identical and is representative of moderate H-bonding systems. **Fig (b)** depicts a symmetric double well potential with a possibility of hydrogen transfer through a high barrier. **Fig (c)** also represents a symmetric double well potential but with a low barrier (sometimes referred as "low barrier hydrogen bond"). In low barrier hydrogen bond (LBHB) case, the hydrogen atom alternates its position between the two acceptor atoms with its average position at the centre. The hydrogen here has a larger span of delocalization and such situation is seen in strong H-bonding systems. If the hydrogen atom is centered between the two oxygen atoms, a single well potential curve develops and the distance between the two acceptors atoms is the shortest as shown in **Fig. (d).**

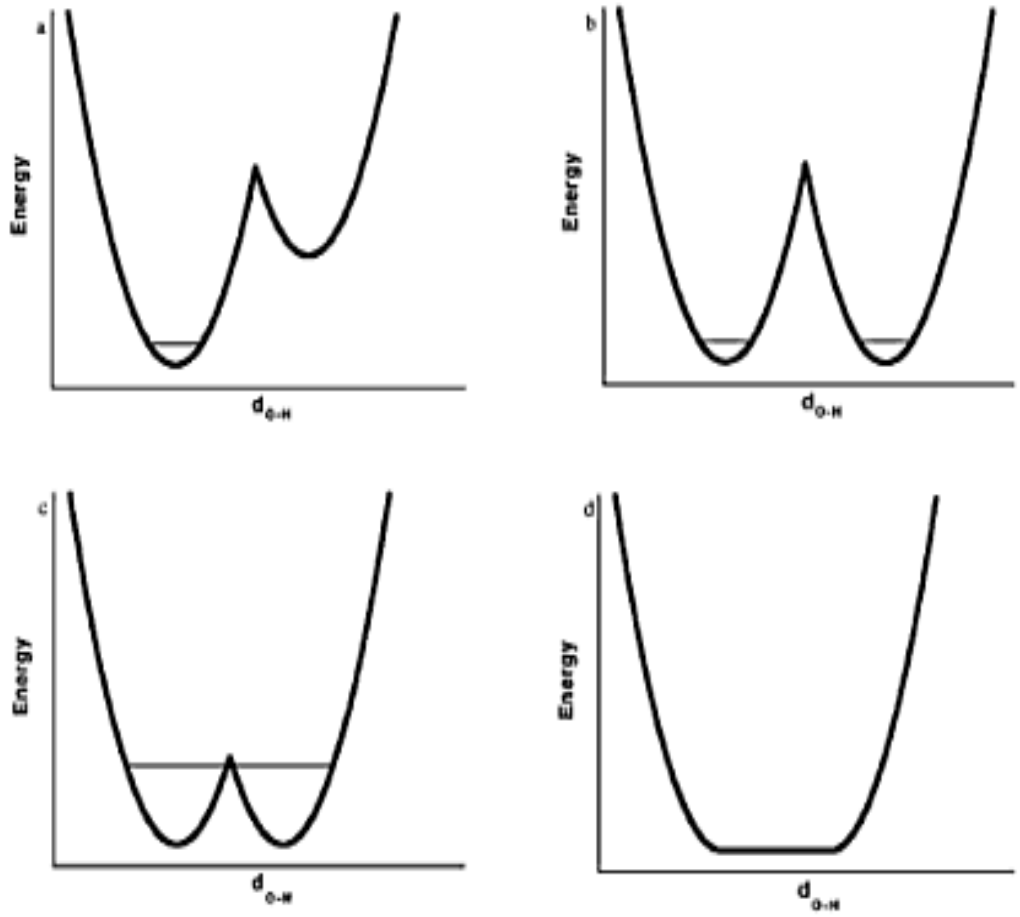

Fig 1. Potential energy curves for OHO hydrogen bonds: (a) asymmetric double well potential, (b) symmetric double well potential, (c) low-barrier hydrogen bond, and (d) single well potential [69].

1.3 Methods of studying H-bonding:

Over the years, several spectroscopic techniques have been employed to study both weak and strong hydrogen bonding interactions including IR spectroscopy, X-Ray and neutron diffraction, 1H NMR spectroscopy. The resulting data are processed to compare various parameters such as bond lengths, bond angles, bond energies and so on. Based on the differences in the bond energies, hydrogen bonds can be classified into three types. The table below presents some notable differences among the three. There is another classification of hydrogen bonds based on 'conventionality' of the donor and acceptor groups. Convention donors include N-H, O-H, X-H (X-Halogen) and S-H and conventional acceptors include these same atoms in the different hybridizations. Weak hydrogen bonds are also non-conventional and most strong bonds are conventional with some exceptions. Generally but not always, these conventional donors and acceptors are fairly acidic or basic. Different techniques are employed for studying a suitable type of hydrogen bond interaction ranging from weak to strong.

1.3.1 Crystal structure analysis

Different methods such as X-Ray and neutron diffraction have been extensively used for studying weak hydrogen bond interactions. Neutron diffraction provides accurate information regarding the position of the hydrogen atom in the hydrogen bonding interaction. X-Ray diffraction, on the other hand gives a measure of experimental charge distribution in crystals through their d-theta plots, operational at low temperatures, thereby providing us with a greater insight on the intermolecular interactions.

1.3.2 Vibrational spectroscopy

Vibrational spectroscopy is typically employed for studying hydrogen bonding interactions in condensed phases. Its study includes all the three types of hydrogen bonding. The vibrational frequency (and the shifts) of the atomic groups involved in hydrogen bonding are used as the probe. One of the major drawbacks of this technique is that the effects of weak hydrogen bonds on vibrational spectra are not always as clear as for strong bonds, and can be quite dissimilar for different kinds of weak hydrogen bond. Also, the study of vibrational spectra does not always distinguish between intra- and inter-molecular effects.

1.3.3 Gas phase rotational spectroscopy

Gas phase spectroscopy is yet another experimental technique for hydrogen bonding studies. Since, the adducts formed here are mainly gas phase, they remain in their ground vibrational state, free of any interference from other molecules. The other main advantage over condensed phase adducts is that apart from geometries, other experimental parameters such as dissociation energies, force constants are easily determined. Moreover, the vibrational behaviour of hydrogen bonds and its geometry between alternative interaction can be easily derived from the rotational spectra. A disadvantage of this methods is that, hydrogen having a low molecular weight, contributes less to the molecular mass in a hydrogen bonded aggregate, and thus brings down the accuracy in the position of these atoms.

1.3.4 Computation

In contrast to most experimental techniques which provide information on equilibrium geometries, computational methods allows one to study domains of the potential energy surface which are far from the equilibrium structure[21]. Theoretical methods provide benchmark values for the intermolecular interaction energies without any complications of solid state or solution environment effects. Other merits include investigation of various parameters such as electronic redistributions that accompany the formation of hydrogen bond, examination of a phenomenon such as polymorphism or crystallization while mapping out interconversion between various geometries. Today most of the computational techniques rely on ab-initio methods rather than semi-empirical mainly because the former gives reliable interaction energies in most cases to various degrees of approximation. Though computational methodologies are limited by the computing power that is available at the time, "*rapid recent advances in computing sector has shown that computational results age much faster than experimental results*" [70].

The current work presents a different technique, namely, Matrix Isolation Infrared spectroscopy for the study of hydrogen bonded complexes. Matrix Isolation Infrared spectroscopy has been extensively used to study molecular interactions and conformational isomerism. One of the primary advantages of this technique is narrow linewidth of spectral features compared with the condensed phase and room temperature gas phase spectra. Identification of adducts is made possible through the use of Fourier

Transform Infrared (FTIR) spectroscopy in conjunction with matrix isolation technique. A detailed description of this technique is provided in the following chapter.

1.4 Status of current research in weak hydrogen bonded interactions:

Enormous amount of research has been carried out on conventional strong hydrogen bonds such as O-H…O, N-H…O and O-H…N because of their importance in DNA and protein stabilization. After the development of technology, study of weak or non-conventional hydrogen bonding such as C-H…O and H-pi interactions has gained importance in the recent years. The commonly studied complexes are those with C-H…X (X represents proton acceptors like O,N,halogen and pi systems) groups.

The first systematic approach was undertaken by Sutor in the early sixties for the study of C-H…O hydrogen bonds in crystals. Ault and co-workers studied the hydrogen bonded complexes of alkynes and alkenes with several oxygen and nitrogen bases using the matrix isolation technique [22,23]. Varied amount of work has been carried out on the hydrogen bonded complexes of Y-H… π in which the hydride acts as a proton donor towards the pi systems of benzene-, acetylene- or ethylene- type systems [24].

Jemmis et al. [25] has performed similar work on matrix isolation infrared and ab initio study of hydrogen bonds formed between acetylene and chloroform. His experiments indicated the formation of a weak C-H…π hydrogen bond between the precursors, where acetylene acts a proton acceptor and the chloroform as the proton donor. In addition, the experimental and computational results also predicted the existence of a secondary interaction between one of the chlorine atoms of chloroform and a hydrogen in acetylene. These two interactions have been shown to determine the structure and the energetics of the acetylene-chloroform complex.

George at al. [26] performed a matrix isolation infrared study of triethyl phosphate with chloroform and its derivatives, CCl_4 and CH_2Cl_2. The adduct formation was identified from a red shift in the phosphoryl (P=O) stretching vibration of triethyl phosphate. The experimental results showed that the interaction chloroform had with triethyl phosphate was van der Waals, and not hydrogen bonding.

Matrix isolation infrared studies of chloroform with Lewis bases such as N_2, CO, H_2O, CH_3CN performed by Fumiyuki Ito [27] have produced some great insights. The experimental results showed a seamless transition from red shifts (for H_2O and CH_3CN)

to blue shifts (For N_2 and CO) depending on the proton affinity of the base molecules. Natural orbital analyses and electronic charge density calculations predicted the C-H…(sigma type lone pair) isomer to be the most stable.

Recently, phenylacetylene in association with different precursors has been extensively used to address the hydrogen bonding behaviour of multifunctional molecules [28,29]. Phenylacetylene has been a molecule of interest because of its diversity of intermolecular structures with various reagents. One more important reason being, the formation of a C-H…X hydrogen bond which is relatively easier with phenylacetylene compared to acetylene because of the slightly lower deprotonation enthalpy of the acetylenic group in phenylacetylene (1551 KJ/mol) than that of the acetylene (1590 KJ/mol) [30]. Patwari and coworkers have studied phenylacetylene interactions with various small molecules such as water, methanol, methylamine and so on looking at the X-H…π (X=O,S,N) interactions [29]. The recent past has also attracted researchers to study π - π stacking as a weak interactions. Patwari et al. studied this interaction with phenylacetylene dimer using IR-UV double resonance spectroscopy and high level ab initio calculation [31].

1.5 Motivation:

Gas phase complexes in contrast to condensed phase complexes provide a great opportunity to investigate the hydrogen bonding patterns in molecules with multiple functionalities. Therefore, it becomes essential to know, a priori, how an individual functional group behaves in presence of a suitable hydrogen bonding partner. Molecules with multiple hydrogen bonding sites provide the platform to investigate competitive hydrogen bonding. Such molecules often form several closely spaced local minima on the potential energy surface of a dimer or complex which becomes challenging to study. Usually, the multiple hydrogen bonding sites throw up a competition between electrostatic and dispersion energy terms in order to maximize the interaction energy.

The present study involves a matrix isolation study of phenylacetylene-D with chloroform and its isotope. Phenylacetylene offers multiple hydrogen bonding sites and therefore acts as a suitable candidate for the study of such weak interactions. The acetylenic C-H stretching vibration of phenylacetylene is an important spectroscopic indicator to understand the interactions present in various complexes. In the C-H stretch region of phenylacetylene spectra, we observe two strong bands at 3325 cm^{-1} and 3343

cm^{-1} instead of a single C-H vibrational band at $3334cm^{-1}$. The splitting is due to the Fermi resonance coupling between the acetylenic C-H stretching vibration with the combination mode of one quanta of the acetylene C≡C stretching mode and two quanta of the acetylenic C-H out of plane bending mode [29]. Hence, any shift in the acetylenic C-H stretching frequency due to complexation would remain hidden in this region. It therefore becomes important to replace the phenylacetylene precursor with its isotope analogue to suppress the Fermi resonance so that the C-D stretch would appear as a single peak thus enabling the observation of the weakly bonded hydrogen bond complexes.

Phenylacetylene has three hydrogen bonding sites, out of which two act as proton acceptors (phenyl-pi and acetylene-pi clouds) and one acts as a proton donor (acetylenic hydrogen) (**Fig 2**). Chloroform on the other hand has only two hydrogen bonding sites with chloroform C-H acting as proton acceptor (**Fig 3**). These two presursors, having multiple hydrogen bonding sites, produce several minima on the potential energy surface.

1.6 Scope and objective of the present work:

Interactions ranging from electrostatic to dispersive have been studied on complexes of phenylacetylene with water and methanol [29]. This thesis will provide a report on the study of possible interactions formed between phenylacetylene-D and Chloroform. Different computational methods have been employed to reveal the possible adducts formed between the two monomers. Experiments using matrix isolation IR spectroscopy have been carried out on this system to build up a corroboration between experiment and computations.

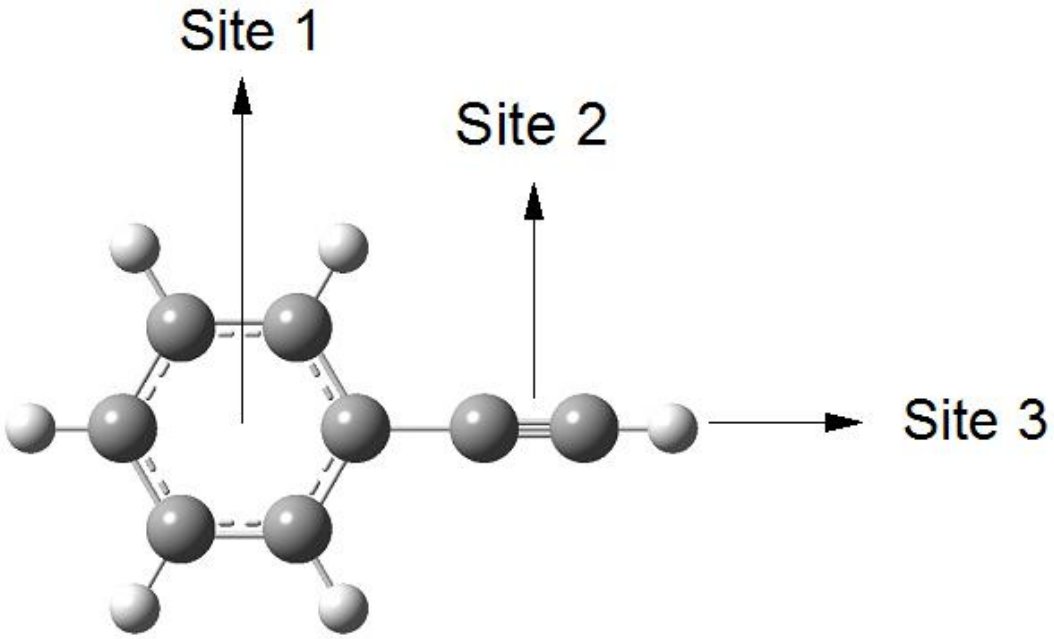

Fig 2. Hydrogen bonding sites in Phenylacetylene

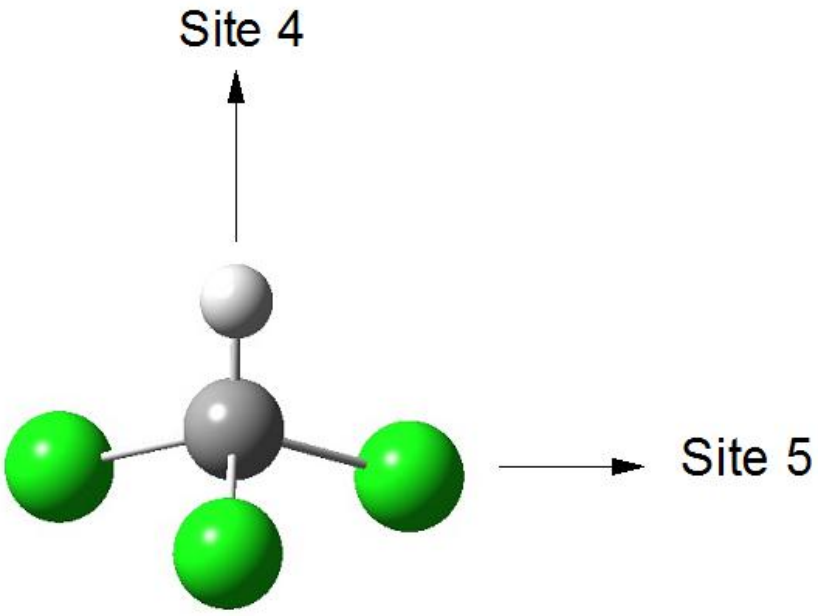

Fig 3. Hydrogen bonding sites in Chloroform

CHAPTER 2

Instrumental and Experimental section

The current section discusses the experimental techniques adopted for the study of hydrogen bonded complexes of phenylacetylene-chloroform followed by computational methods adopted to corroborate the experimental results.

2.1 Matrix isolation (MI) technique:

Coined by George Pimental along with George Porter [32], the term "matrix isolation" refers to a method whereby a substrate is mixed with a large excess of an unreactive host gas and is condensed on a surface that is sufficiently cold to assure rapid solidification of the material. In this way, one obtains a sample where an individual substrate molecule is immobilized in a cavity surrounded by one or more layers of inert material and is thus "isolated" from other substrate molecules in a "matrix" of the host gas. As a consequence of getting trapped in a rigid host material, the guest molecules are thereby prevented from undergoing diffusion. The matrix gas molecules being inert avoid any interaction with the guest species thus increasing their lifetime. And so it becomes advantageous to study reactive intermediates such as radicals, ions or other transient species apart from stable species. Though the study of reactive intermediates in frozen solutions are often referred to under the heading of "matrix isolation", more appropriate term would be "low temperature spectroscopy in rigid media". Several properties of the reactive species after being trapped in inert gas matrix can be easily studied by spectroscopic techniques such as infrared, UV-Visible, microwave, electron spin resonance spectroscopy. This technique serves as a powerful tool to study weakly bound complexes and conformations of molecules.

Generally in the matrix isolation technique, the guest molecules are mixed with matrix atoms in the ratios ranging from 10^3:1 to 10^5:1 so as to achieve isolation. Typically used matrix gases in this technique are nitrogen and inert gases such as Ar, Xe. Apart from offering chemical inertness, a matrix material mist also satisfy some important properties such as low volatility at the temperature of study of interest, optical transparency in the region of interest, low latent heat of fusion and acceptable thermal conductivity. The sketch below presents a schematic picture of the matrix isolation technique in the "proper" sense of the word.

2.1.1 Why Matrix Isolation?

In order to study species that are only of fleeting existence under ambient conditions, one could either look at them very quickly (i.e immediately after the formation) or one could attempt to trap them under circumstances where they can be studied leisurely. The former method would provide kinetic information of the reactive intermediate using time-resolved techniques, but often at the expense of spectroscopy detail, whereas the later methodology can yield much more detailed insight into the electronic and the molecular structure of reactive intermediate.

The chemical properties of the reactive intermediates is liable to change since they are being transferred from their "natural" environments, where they occur as fleeting intermediates on the way from reactants to products, to an "artificial" environment. So, one usually tries to create an environment that provides for minimal interaction with the target reactive intermediate, a goal that cannot be achieved with frozen solvents. Nobel gases, nitrogen, methane or other inert molecular hosts serve as the best choices for this purpose.

Other disadvantage of frozen solvents is that they are often opaque throughout wide region of the infrared and part of the UV spectral range. Since vibrational spectroscopy can provide much more structural informational than UV-Vis spectroscopy, it becomes important to study the reactive intermediates in a medium that allows their observation in IR. Moreover, being entirely transparent in the IR region, all atomic and homonuclear diatomic gases serve ideally as matrix host from this spectroscopic point of view. Another major advantage offered by these materials is that they offer generally much higher spectral resolution (i.e narrow bands) than frozen solvents helping in the disentanglement of complex spectral patterns. A third advantage offered by matrix isolation over frozen

solvents is that the reactive intermediates must not necessarily be generated in situ, but can be made by flash vacuum pyrolysis or in plasma processes prior to their quenching with an excess of the host gas on the cold surface. Finally, since the gaseous molecules are solidified at low temperatures where unimolecular thermally activated processes are largely suppressed, the reactive intermediates get stabilized.

2.1.2 Limitations of Matrix Isolation:

The first limitation of this technique is on the size of the species being studied and/or its thermal lability since the precursor of the reactive intermediate to be studied must be an isolable substance and vaporizable without decomposition. Second, reactive intermediates produced from biomolecular attacks (such as nucleophiles, electrophiles, oxidants or reductants) which normally occurs in solution phase are generally unavailable in the context of matrix isolation. The only reactive intermediate studied by matrix isolation are accessible by means of unimolecular processes (fragmentation, ionization) induced by external energy sources. Third, precursors that readily yield some reactive intermediates in solution or gas phase, will not necessarily "work" inside a matrix because of the cage effect. Thus, even after getting photocleaved in solution or in gas phase, a precursor may appear to be entirely photostable under matrix conditions, simply because the fragments recombine immediately after their formation. A fourth problem is that the noble gas matrices are notoriously poor heat sinks (meaning that molecules absorb minimal heat) because of very low energy, lattice phonons (a quantum mechanical term for normal mode vibration). This leaves excess amount of energy in the surrounding which evokes other chemical processes. The excess energy imparted onto the formation of a nascent reactive intermediate gets dissipated in secondary chemical processes such as rearrangements or fragmentations due to slow thermalization compared to solution. Finally, taking lower host/guest rations may complicate the spectra simple because polar substrates have a tendency to form dimers or higher aggregates. Going to higher host/guest rations may eliminate aggregation of precursors but at the cost of spectroscopic signal intensity.

2.2 Matrix effects:

In order to properly interpret the infrared spectra of matrix isolated species, one needs to understand various effects that the matrix can have on the vibrational feature of the analyte. The perturbation of the vibrational potentials of analyte due to the analyte-matrix

interaction contributes the most among the various matrix effects. These interactions can result in either a shift in the frequency relative to isolated gas phased molecules, or splitting of the vibrational bands. The major interactions contributing to the frequency shift ($\Delta\nu$) are from electrostatic ($\Delta\nu_{elec}$), inductive ($\Delta\nu_{ind}$), dispersive ($\Delta\nu_{dis}$) and repulsive ($\Delta\nu_{rep}$) terms, given by expression,

$$\Delta\nu = (\nu_{matrix} - \nu_{gas}) = \Delta\nu_{elec} + \Delta\nu_{ind} + \Delta\nu_{dis} + \Delta\nu_{rep}$$

Where, ν_{matrix} and ν_{gas} represents the frequencies of the vibrational mode in the matrix and gas phase respectively [33].

In solution phase, the frequency shifts are dominated by perturbations arising due to the solvent interaction whereas the long-range London dispersion forces and short range repulsive forces dominate in the inert gas matrix. The frequency shift, $\Delta\nu$, in solutions is given by the Buckingham expression [34],

$\Delta\nu = (\nu_{solvent} - \nu_{gas}) = [B_e/hc\omega_e]\,[U'' - 3AU'/\omega_e)$

Where, $B_e = h/8\pi^2\mu c r_e^2$, is the rotational constant,

A is the anharmonicity constant,

$U' = \{\delta U/\delta r_{bc}\}$ and $U'' = \{\delta^2 U/\delta r_{bc}^2\}$

$c\omega_e$ is the harmonic oscillator frequency for the normal vibration, Q.

Using this expression the frequency shift of the molecule in a matrix can be explained. **Fig 4**. shown below considers a situation with a triatomic molecule trapped in a matrix cage with frequency shift represented by the potential energy curves. It can be seen from the plot that when R_{cm} (distance between the matrix atom and one of the atoms of the trapped molecule) is larger than R_e (equilibrium distance), U' and U'' are negative and since A is also negative, $\Delta\nu$ becomes negative. When R_{cm} is less than R_e, U' and U'' become positive leading to a positive $\Delta\nu$. In case of a larger molecule, where $R_{cm}<R_e$ the molecule experiences a "tight cage" effect giving rise to a blue shift and in case of a smaller molecule, where $R_{cm}>R_e$ the molecule experiences a "loose cage" effect leading to a red shift. Pimentel and Charles have reported that for a trapped molecule in a matrix, the high frequency stretching vibrational display negative shift as in a loose cage and the low frequency stretching and bending vibrations display positive shifts as in a tight cage [35]. So, in less reactive environment, the high frequency modes will shift to lower frequency and low frequency modes will shift modes will shift to higher frequency.

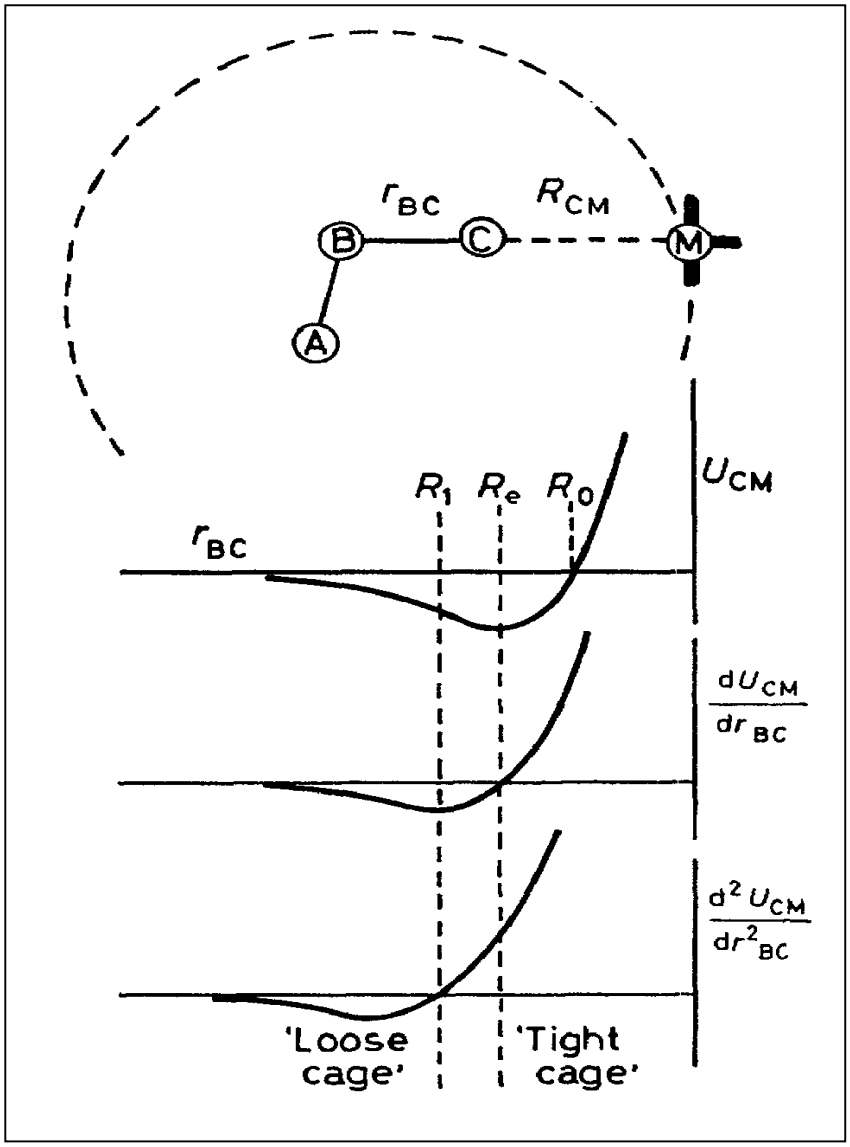

Fig 4. Potential energy curves for a triatomic molecule trapped in a matrix [35].

Following are various other factors contributing to the multiple band structures for a particular vibration bond in matrix:

2.2.1 Rotation effects in a matrix cage:

When a molecule gets trapped inside a cavity, its rotations may or may not get hindered in the noble gas matrix, depending on the cavity size. As result, a number of small molecules such as H_2O, NH_3, OH- and HX (X=F,Cl) tend to rotate in noble gas matrix [33]. Evidences show that molecules that rotate in one matrix may not rotate in another matrix [36]. Rotational features can be identified by reversible intensity changes on temperature cycling unlike splitting due to matrix site effects which are not reversible on temperature cycling.

2.2.2 Multiple trapping site effects:

In an array of inert atoms, an analyte molecule may be trapped in different types of sites in the matrix. Depending upon the type of lattice, different perturbations in the vibrational potential would lead to splitting in vibrational features. Trapping of guest specied can occur either in a substitutional site or an interstitial site. Generally, noble gases, except helium, crystallize in face centrered cubic (FCC) lattices where a single atom is surrounded by 12 nearest atoms. A substitutional site can accommodate a guest molecule of spherical diameter $r/\sqrt{2}$ (where r is the radius of the matrix sphere). Studies have shown that accommodating a molecule of reasonable size requires more than one substitutional site [58]. Although, a molecule is highly likely to get trapped in a substitutional site in a FCC lattice, some find their way into interstitial sites too. There are two types of interstitial sites. Tetrahedral site (which has four nearby atoms) and octahedral site (surrounded by six nearby atoms). A guest molecule with a spherical diameter 0.159r and 0.293r can be accommodated in a tetrahedral and an octahedral sites respectively [59]. The intensity of shifts in the vibrational modes varies according to the stability of the trapping sites. The bands arising due to the species trapped in the unstable sites can be made to vanish by annealing the matrix at elevated temperature (~35K). The problem of unstable sites could also be solved/studied by varying the rates of deposition and by isolating the molecules in a different matrix.

2.2.3 Aggregation:

Matrix Isolation experiments typically employ matrix/analyte (M/A) ratios of 1000:1, where true isolation of analyte can be achieved. Usage of low M/A ratios lead to the formation of molecular aggregates in addition to monomers. Features arising due to self-association can be identified from their concentration dependence and from warm up experiments in which formation of dimer and higher multimers occur due to diffusion. Significant changes in the spectrum can occur of two species are trapped nearby leading in overlap of the cages. Probability of maximal isolation of the analyte molecules can be calculated considering an example of carbon monoxide (CO) molecule. The probability of interaction of a CO molecule occupying a single substitutional site is the same as the chance of finding another molecule among the 12 sites forming the cage. The chance for the absence of the second CO molecule is given by the formula, $P=(1-r)^{12}$, where r is the reciprocal of the matrix ratio. The expression reduces to P=1-12r for very small values of r. Hence, in order to ensure 99% isolation, the matrix ratio should be of the order of 1000.

2.2.4 Lifting the degeneracy of vibrational levels:

A molecule trapped in a particular site may experience different frequency shifts depending upon the symmetry of the site occupied. Molecules having degenerate modes of vibration undergo shifting in the presence of asymmetric sites, resulting in the splitting of the vibrational features, such as that observed in CO_2 [52-54] and C_2H_2 [55,56]. The presence of nitrogen as an impurity in argon matrix give rise to additional bands for a wide range of solutes.

2.3 Matrix isolation infrared setup:

A typical matrix isolation infrared setup comprises of four major components namely, cryostat, Vacuum system, sample introduction system and FTIR spectrometer. **Fig 5** Shows a photograph of the matrix isolation setup installed at IISERM. Presented below is a brief description of each one of the major components.

2.3.1 Cryostat based on a closed-cycle helium compressor:

A helium compressor based cryostat basically comprises of four main parts,

1). Cold head

2). A helium compressor

3). A temperature control unit

4). A optical extension set

1). ***Cold head and compressor:***

The compressor is the most important unit in a matrix isolation setup which attains temperature as low as 10K. A closed cycle cryostat operates on the principle of Gifford-McMahon (GM) refrigeration cycle. The compressor (Sumitomo cryogenics, Model No: HC-4E1) is connected to a cold head through two gas inlets. While one inlet supplies high pressure helium gas to the cold head, the other inlet returns low pressure helium gas from the cold head. The flow rate of the helium gas from through the high pressure inlet is controlled by the compressor in order to obtain the desired refrigeration capacity. The heat generated due to compression of the gas of compression of the gas of compressor is removed by a 3KW chiller. A photograph of compressor and chiller used in the present study is shown below in **Fig 6**.

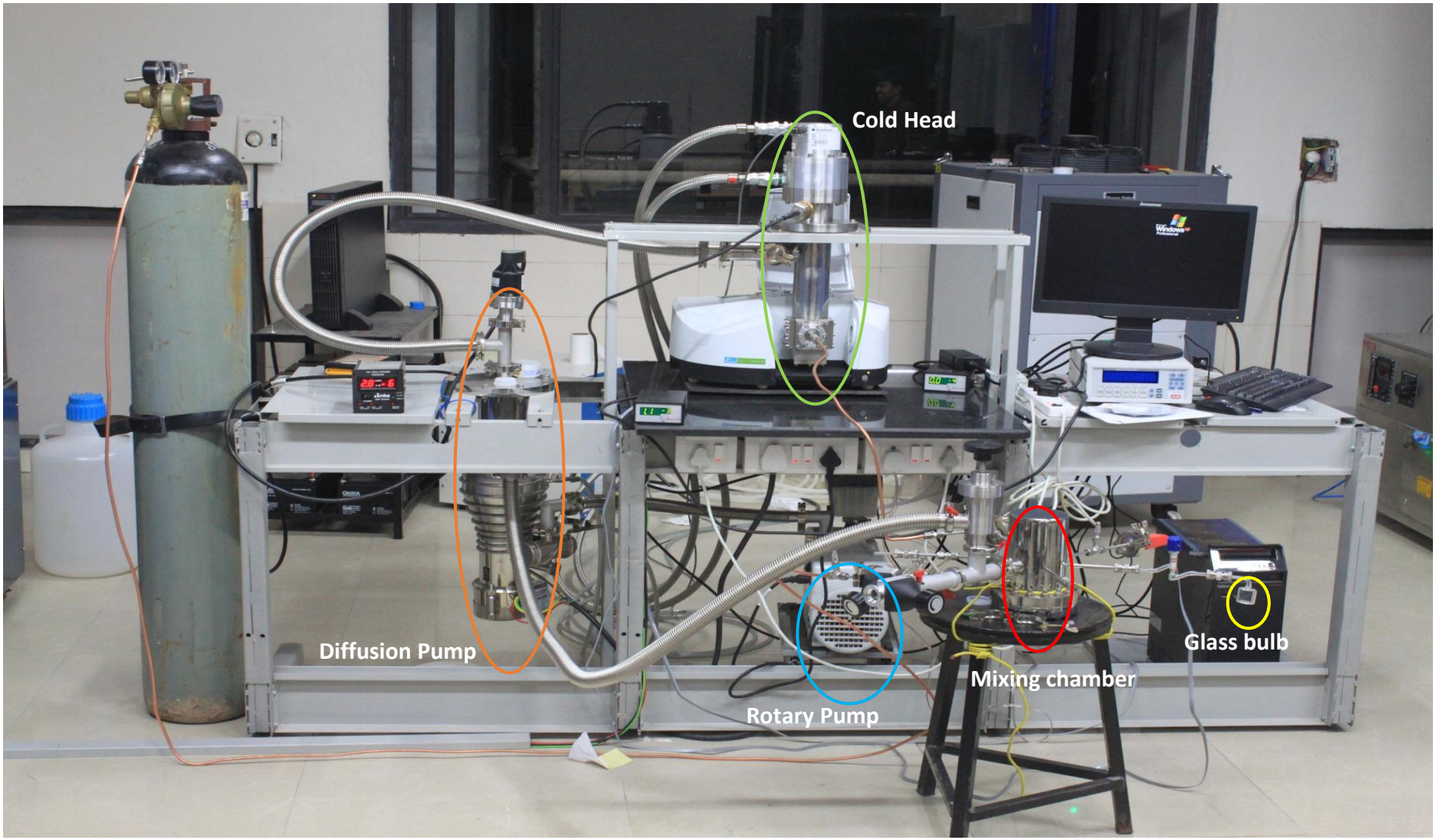

Figure 5. Matrix Isolation infrared setup installed at IISER Mohali

Figure 6. Photograph of Compressor and Chiller

Working principle:

The Gifford-McMahon (GM) cycle was originally proposed in the early 1960s as a regenerative cycle that could potentially reach the helium temperature range [57]. The cold head comprises of a regenerator, a displacer and a compression and expansion space. With the displacer at is lowest position and the outlet (return) valve closed, the inlet (high pressure) valve is opened to fill the regenerator and space above the displacer. The displacer is moved to its upper position and the high pressure gas passes through the regenerator and is cooled isobarically by the matrix, with the inlet valve still open. Next, the inlet valve is closed and the outlet valve is now opened. The gas in the regenerator and cold space below the displacer undergoes expansion, which produces refrigeration. Finally, the displacer moves back to the lowest position and the low pressure cold gas is warmed isobarically by the matrix refilling the space above the displacer at room temperature [57]. **Fig 7** shows a pictorial description of the GM refrigerator.

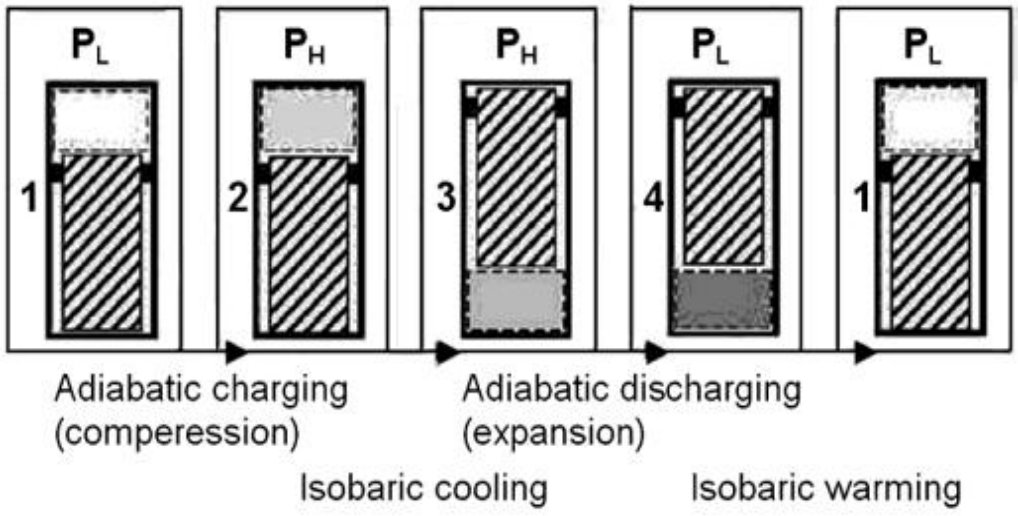

Fig 7. Cycle description for the GM refrigerator [57].

2). ***Temperature Control Unit:***

Annealing process in the matrix is performed to promote diffusion of the trapped species and to examine the presence of multiple sites arising from unstable matrix sites. This is achieved through a temperature controller unit (Lakeshore 335 with PID

controller) which regulates temperatures from 12K to 300K using a heater mounted on the cold tip of the cryostat.

Low temperature measurements are generally done using four thermometric methods: Thermocouples, solid state thermometers, capacitance cryogenic temperature sensors, hydrogen vapour pressure thermometers. In our cryostat, the temperature is measured with the help of silicon diode sensor.

3). ***Substrate holder or optical extension unit:***

The extension unit comprises of a substrate holder, a radiation shield and a rotatable vacuum jacket. A KBr substrate of 25mm diameter and 4 mm thickness is mounted on the substrate holder, attached to the cold head. The vacuum jacket, which contains two KBr windows of 40mm diameter and 4mm thickness transmits infrared beam to the detector through KBr substrate. The third port is fitted with a quartz window for viewing purposes. The fourth port has a flange to which a sample inlet is connected to carry out the deposition process.

2.3.2 Vacuum system:

Necessary vacuum in the cryostat was attained by an oil diffusion pump (Edwards, Diffstack MK2 series 100/300) with a pumping speed of 280 litres/sec, backed by a rotary pump (Edwards) with a pumping speed of 100 litres/sec. A second rotary pump (Hind Hivac Model No. ED6) was used as a roughing pump for the vacuum system. Pressure achieved using these two pumps was ~10^{-6} mbar which was measured using a cold cathode gauge (Model No: MKS 943). The pressure above 10^{-3} mbar was measured using a Pirani gauge (Edwards APG 100 Active Pirani Gauge).

2.3.3 FTIR spectrometer:

The infrared spectrum of absorption and emission of the complexes were obtained using a Perking Elmer FTIR spectrometer which works on the principle of Michelson interferometer. The spectrometer recorded the spectrum from 400-4000 cm^{-1} with a resolution of 1 cm^{-1}.

2.3.4 Sample Introduction system:

Sample can be introduced into the vacuum system either through a single effusive nozzle or through a double jet nozzle system. The latter is used when the sample

to be deposited has a low vapour pressure. Analyte and the matrix were mixed in a stainless steel mixing chamber of one litre capacity, and the mixture was introduced into the vacuum system through a single effusive nozzle.

2.4 Experimental procedure:

Samples were loaded into small glass bulbs connected to the mixing chamber. Thorough degassing of the bulbs was performed prior to the loading so as to avoid any impurities. The samples were subjected to several freeze-pump-thaw cycles before use. The amount of the sample deposited in a given experiment was controlled by adjusting the vapour pressure of the sample. This was achieved by maintaining the sample at the required temperature for about an hour in an ethanol-liquid nitrogen slush bath, to obtain the desired vapour pressure of the sample. A platinum resistance thermometer was used to measure the temperature of the slush bath. The desired amount of the sample was let into a stainless steel mixing chamber of one litre capacity. The chamber was then filled with matrix gas to get a desired M/A ratio. The mixture was allowed to stand for 15 minutes for thorough mixing. The mixture was then allowed to stream into the vacuum system for deposition on to the cold KBr substrate. The rate of deposition was controlled with the help of a fine needle valve (Pfeiffer Vacuum, D-35614 Asslar, EVN 116, No. PFI32031).

2.5 Computations:

Ab initio computational calculations were carried out using the GAUSSIAN 09 [37] package on a Linux operating system. Computations were done to arrive at molecular properties such as structures, energies and frequencies for corroboration with our experimental results. The nature of the interactions between the precursors of the complexes were studied using AIM package [38]. Various literatures have produced a detailed treatment of ab initio calculations [39-45]. A brief discussion regarding computations is given below.

2.5.1 Geometry optimization and frequency calculation:

In order to determine the structure of a molecule corresponding to a minimum on the potential energy surface, one needs to optimize the input geometry. A guess molecular structure is specified as an input. The energy and gradient values are calculated at the point on the potential surface corresponding to this initial geometry. This information is

used to determine how far and in which direction should the next step of geometry optimization be so as to improve the geometry. A structure is minimized when it attains an equilibrium, i.e the forces are zero. The optimization in Gaussian was achieved when the forces, root mean square of forces, the calculated displacement and the root mean square of the displacement for the subsequent step are below a preset threshold value.

A variety of levels of theories are available for performing optimization calculations. Some of them are: Hartree-Fock methods (HF), Density Functional Theorem (DFT), Møller–Plesset perturbation theory (MP_n) (where n denotes the order of perturbation), Configuration interaction (CI), Coupled cluster (CC), Multi-configurational self-consistent field (MCSCF), Multi-reference configuration interaction (MRCI). Optimization calculations in the present study were carried out using Density functional methods (B3LYP) and Minnesota functions (M06-2X) using 6-311++G** basis. The B3LYP method uses the Becke three parameter non-local exchange functional[46,47] with non local correlation of Lee et al.[48]. The Minnesota (M06) suites of functionals are set of four meta-hybrid GGA DFT functionals (generalized gradient approximation (GGA) in which the density functional depends on the up and down spin densities and their reduced gradient) which are believed to reproduce dispersion forces rather well[49,50].

Vibrational frequency calculations were performed at the same level of theory used for geometry optimization. Vibrational features were assigned to the computed structures corresponding to minima on the potential surface using the vibrational frequency calculations. The computed vibrational frequencies were scaled for the purpose of comparison with the experimental results. The scaling factor was calculated by correlating the strongest feature indicated by the computations in the spectral region of interest with the experimentally observed strongest feature. This scaling factor was then used to scale all other vibrational frequencies thereby bringing the computed frequency in good agreement with that of the experiment. The computed scaled spectra were used to simulate vibrational spectra. The synthetic spectra assumed a full width at half maximum (FWHM) of 1 cm^{-1}, which is the typical resolution of our instrument. Vibrational frequency calculations also produced Zero point energy (ZPE) values which were used to calculate ZPE corrected energies.

2.5.2 Stabilization energy calculation of complexes:

The following approach was invoked to compute the stabilization energy of the complex. The stabilization energy of a complex is given by

$$\Delta E = E_{AB} - (E_A + E_B)$$

where, E_A, E_B and E_{AB} represent the energies for the monomers A, B and complex AB respectively. The above expression shows that the complex tends to stabilize for a negative value of ΔE. In the following discussions, only the magnitude of ΔE will be given with negative sign being implied by the use of the term stabilization. The stabilization energy of the complex corrected for zero point energy (ZPE) was also calculated.

The ZPE vibrational energy is equal to one half the sum of the vibrational fundamental frequencies. It can be seen through a simple example that a complex has six normal modes more than the sum of the normal modes of the two monomers. Assuming non-linear molecules with the two monomers having N1 and N2 atoms respectively, the complex will have (N1+N2) atoms. The number of additional normal modes can be calculated as follows,

Extra normal modes = $\{3(N_1+N_2)-6\} - \{(3N_1-6) + (3N_2-6)\} = 6$

The calculation of the energy of a complex (E_{AB}), uses both the basis functions of the monomers, while the energy of the individual precursors (E_A and E_B) are calculated using the basis functions pertaining only to the corresponding precursors. Since the computation of the complex uses a larger number of basis functions, the energy obtained will be lower, as basically each monomer can use the basis functions of other. Stabilization energies thus derived from the calculated energies E_A, E_B and E_{AB} will be overestimated and the error is referred to as the basis set superposition error (BSSE). BSSE does not have an easy way of correction despite being well understood. The best way of eliminating BSSE is by increasing the basis set until the stabilization energy reaches to the desired accuracy. This implies large computation times for even small systems. The commonly employed method for BSSE problem is by counterpoise correction proposed by Boys and Bernardi [51]. This scheme calculates the energies of the monomers and the complex in the same basis set spanned by the complex. The difference is calculated as follows,

$$\Delta E = E_{AB}(AB) - \{E_A(AB) + E_B(AB)\}$$

where, $E_A(AB)$ = Energy of the monomer A using the basis set AB

E_B (AB) = Energy of the monomer B using the basis set AB

E_{AB} (AB) = Energy of the complex AB using the basis set AB

The present study also accounts for the BSSE correction term in calculating the stabilization energy of the complex, evaluated as follows:

BSSE correction = $\{E_A(A) - E_A(AB)) + (E_B(B) - E_B(AB)\}$

Where, $E_A(A)$ = Energy of the monomer A using the basis set A

$E_A(AB)$ = Energy of the monomer A using the basis set AB

$E_B(B)$ and $E_B(AB)$ are also defined similarly.

The BSSE correction term turns out to be a positive quantity and so the overall BSSE corrected energy terms have a lesser negative value. Corrections in energies from ZPE and BSSE were not included simultaneously as these values tend to overcorrect the stabilization values [51].

2.5.3 Atom in molecules (AIM) calculations:

"*The molecular structure hypothesis- that a molecule is a collection of atoms linked by a network of bonds, was forged in the crucible of the nineteenth century experimental chemistry*" [68]. To understand and get more information about a molecule and its atoms computationally, Bader proposed the theory of atoms in molecules, which uses an analysis of the electron density topology[67]. "The theory recovers the central operational concepts of the molecular structure hypothesis, that of a functional grouping of atoms with an additive and characteristic set of properties, together with a definition of the bonds that link the atoms and impart the structure".

Quantities obtained from the electron density plots are bond critical points, charge density (ρ), Laplacian of charge density ($\nabla^2\rho$), which is also the trace of Hessian of ρ. The charge density, $\rho(r)$, is a scalar field defined over three dimensional space and has a definite value at each point in space. A critical point in a space is defined at a maximum, a minimum, or a saddle point, where the first derivative of $\rho(r)$ vanishes. Whether a function is maximum or minimum at a point is decided by the sign of its second derivative or curvature at this point. The critical point is generally described in terms of two variables: ω and σ. The symbol ω, denotes the number of non zero eigenvalues or non zero curvature of ρ at the critical point, and is called the rank of critical point. The symbol σ, denotes the algebraic sum of the signs of the eigenvalues. A critical point is represented as (ω, σ). For example, a (3,-1) critical point represents three non-zero curvatures with one positive and two negative eigenvalues. A (3,-1) critical point

typically corresponds to a bond between two atoms, a (3,+1) corresponds to a ring, (3,+3) corresponds to a cage and a (3,-3) corresponds to a maximum. The number of critical points of all types, which can coexist in a system with a finite number of nuclei, are governed by the Poincarè-Hopf relationship,

$$n- b+ r- c= 1$$

where, n is the number of nuclei, b is the number of bond critical points, r is the number of ring critical points and c is the number of cage critical points.

The Laplacian of charge density, $\nabla^2\rho$, which is the sum of the three Hessians at a bond critical point, provides a useful characterization of the manner in which the electron charge density is distributed in the inter nuclear region. In a covalent interaction, where the interaction is of shared type, the curvature and values ($<10^{-1}$ au) of charge density are large, Laplacian of charge density may be positive or negative usually in the same order of magnitude as ρ. For hydrogen bond complexes, and other closed shell interactions such as van der Waals complexes and ionic systems, the charge density ($\sim10^{-2}$ to 10^{-3} au) has a lower value at the bond critical point and the Laplacian of the charge density is positive.

CHAPTER 3

Results and Discussion

3.1 Introduction:

Chloroform has one hydrogen atom and three chlorine atoms attached to a carbon atom giving the molecule a possibility of forming hydrogen bonds from two different sites. The single hydrogen serves as a proton donor while three chlorine atoms serve as proton acceptors.

On the other hand, phenylacetylene-D (PhAc-D) has two different sites which can act a proton acceptors, the benzene π cloud and the acetylenic π cloud and one site i.e the acetylenic hydrogen which can serve as the hydrogen donor.

Interactions between chloroform with HF have been investigated and the results have shown two types of hydrogen bonded complexes, one involving the hydrogen of $CHCl_3$ and another involving the hydrogen of HF [60]. Similar studies have also been carried out with $CHCl_3$-acetylene and $CHCl_3$ - triethyl phosphate [61] complexes where $CHCl_3$ is shown to act as a Lewis acid [61].

It therefore becomes interesting to extend such study to the PhAc-D – $CHCl_3$ complex in order to better understand the nature of specific interactions of weak non polar bonds.

Theoretical methods:

The computational calculations on the complexes and the monomers were performed using the GAUSSIAN 09 program. The fully optimized geometries and the vibrational frequencies were calculated using Minnesota functional (M06-2X) and B3LYP hybrid functional of the density theory (DFT), in conjunction with 6-311++G (d,p) basis sets. The stabilization energies of the complexes were calculated at each of

these levels of theory. Separate calculations of ZPE and BSSE corrected stabilizing energies were also obtained as described earlier with ZPE correction calculated as,

$\Delta E_{ZPE} = \Delta E_{CAL} + ZPE$

The frequency calculations obtained at various levels of theory assured that the optimized geometries were indeed a minimum on the potential surface and were used in assigning various features observed in the experiments. Appropriate scaling factors were added to the computed frequency values so as to bring in an appropriate correlation between the experiment and the calculated data. Atoms in Molecules (AIM) calculations were also performed on each of the complexes separately to examine the charge density topology. (3,-1) critical points were located in each case. The electron density, $\rho(r)$ and Laplacian of electron density $\nabla^2\rho(r)$ were computed for the critical points. Apart from this, solvent effects were also incorporated into the energy and frequency of the monomers and complexes at a later stage to look at possible changes in their values in different matrix environments.

Experimental Details:

All the experiments performed with the matrix isolation set up were using either Argon or in Nitrogen matrix. Argon condenses at 83.81K and so it forms a rigid matrix at 12K. Similarly, Nitrogen condenses at 77K and is also rigid at 12K [62]. The annealing temperature was different for both the gases. The annealing temperature was restricted to 35K in the case of Argon and to 32K in the case of Nitrogen, since the matrix is presumed to decompose at temperatures beyond this.

The features newly observed in the experiments were affirmed by concentration dependent experiments. The PhAc-D: Chloroform:Matrix concentrations used for the present study were 1:5:1000, 1:10:1000, 3:6:1000, 3:10:1000, 6:6:1000. Apart from the complex studies, the individual spectra of PhAc-D and Chloroform monomers were also recorded at different matrix to sample ratios. Since the concentrations of the analyte was low, annealing was performed so as to let molecules diffuse inside the matrix. The experiments based in Argon required annealing time of 7 hours while the experiments in Nitrogen annealed for 3 hours proved sufficient. The spectra observed from the experiments were deconvoluted so as to distinctly identify the shifted features. The Gamma value for every deconcolution process was kept constant at the value of 1.

It is important to note that every experiment performed will have features of water complex innately in it. The reason being the presence of moisture in the vacuum system.

3.2 Results and Discussion:

3.2.1 Experimental:

As mentioned earlier, the PhAc-D and Chloroform experiments were carried out in both Ar and N_2 matrices, separately. **Fig 8 (a)** shows the spectra obtained when Phac-D and chloroform were co-deposited in the Argon matrix while **Fig 8 (b)** shows the co-deposited PhAc-D and chloroform in Nitrogen. The spectrum obtained when PhAc-D alone was deposited in the Argon matrix is also shown in the **Fig 8 (a & b)**. The spectral region depicted in this figure is between 2500 and 2700 cm^{-1}. In this spectral region, PhAc-D has a strong absorption at 2607 cm^{-1} which is attributed to the C-D stretch of the PhAc-D molecule. Another feature appears at 2599.15 cm^{-1} in all except chloroform alone spectra. This feature appears due to the site effect in the argon matrix. Upon annealing, this feature is seen to diminish in its intensity.

When PhAc-D and chloroform were co-deposited and the matrix then annealed, a new absorption feature appeared at 2595.14 cm^{-1}. This band appears only on co-deposition of the reagents and its intensity is increased as the concentration of either of the two reagents were increased. This feature could be possibly be due to complex formation. Since, low concentration of the reagents were used, we believe that this band is due to the formation of a 1:1 complex of PhAc-D and chloroform.

In the Nitrogen matrix, PhAc-D has a strong absorption at 2598.05 cm^{-1} assigned to the C-D stretch of PhAc-D as shown in **Fig 9 (a & b).** The complex feature of PhAc-D and chloroform appeared at 2584.56 cm^{-1} which also increases in intensity as the reagent concentrations are increased.

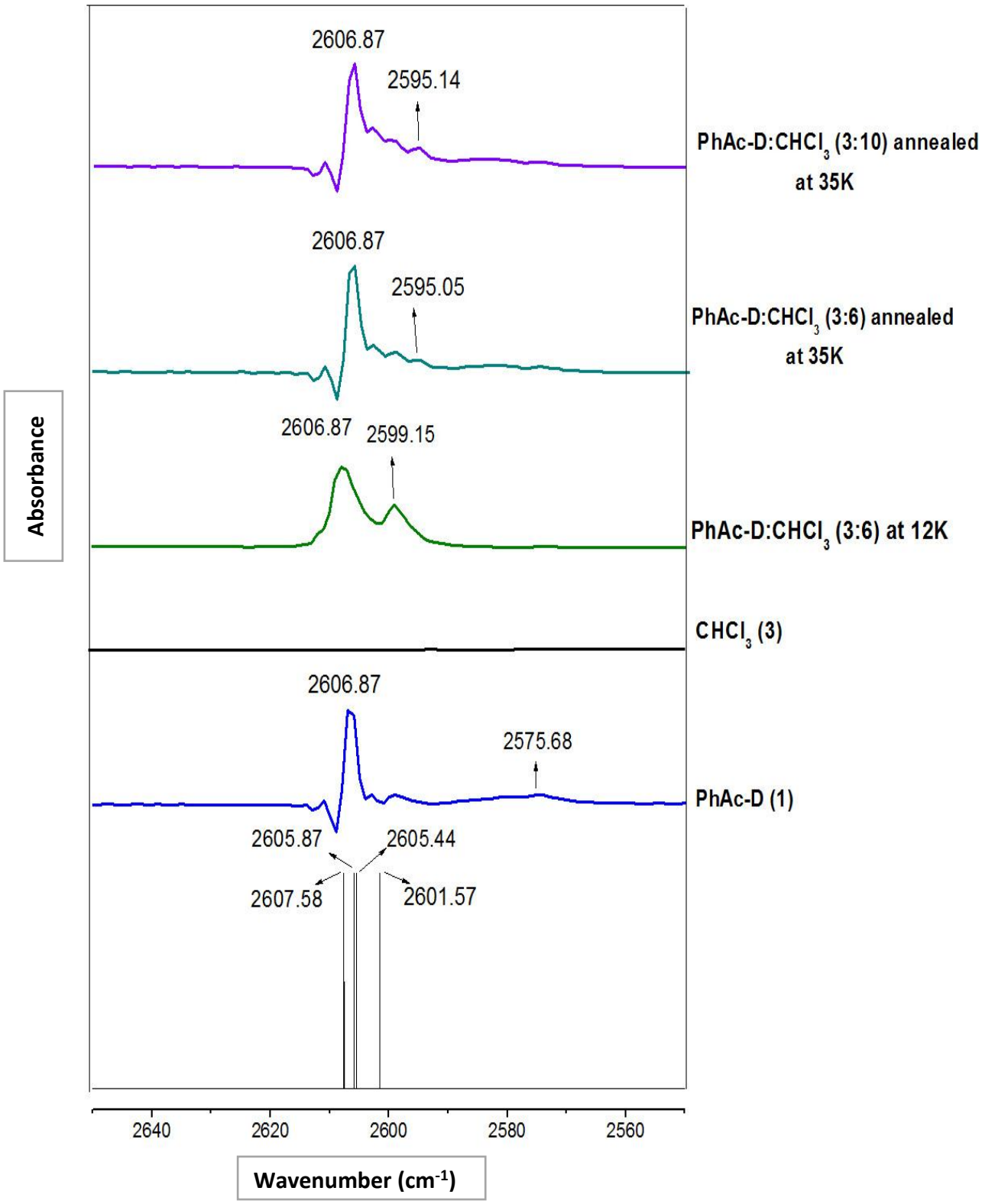

Fig 8 (a). Spectrum of PhAc-D and PhAc-D – $CHCl_3$ complexes in Argon matrix and its comparison with computed frequency at B3LYP/6-311G++ (d,p)

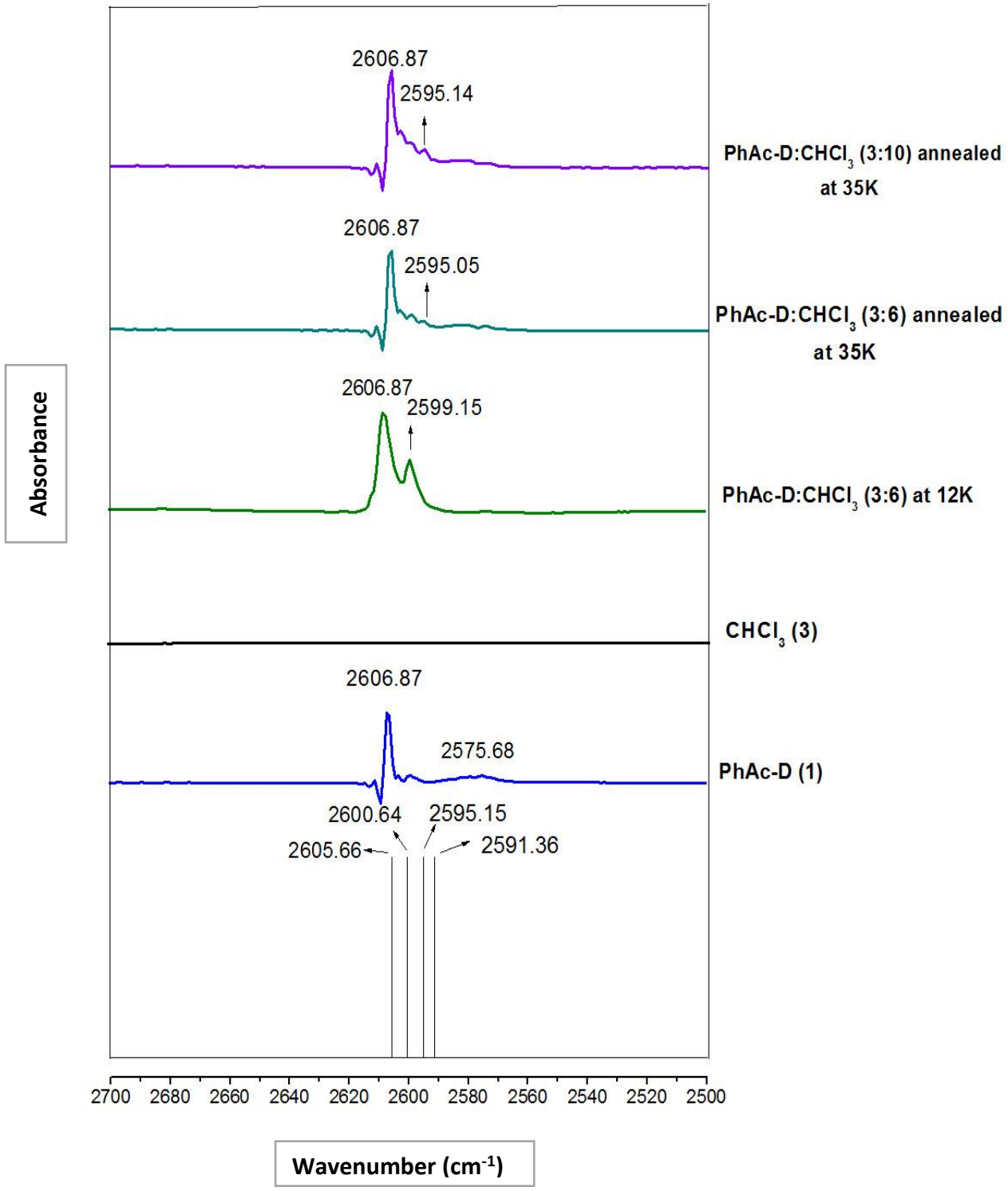

Fig 8 (b). Spectrum of PhAc-D and PhAc-D – $CHCl_3$ complexes in Argon matrix and its comparison with computed frequency at M06-2X/6-311G++ (d,p)

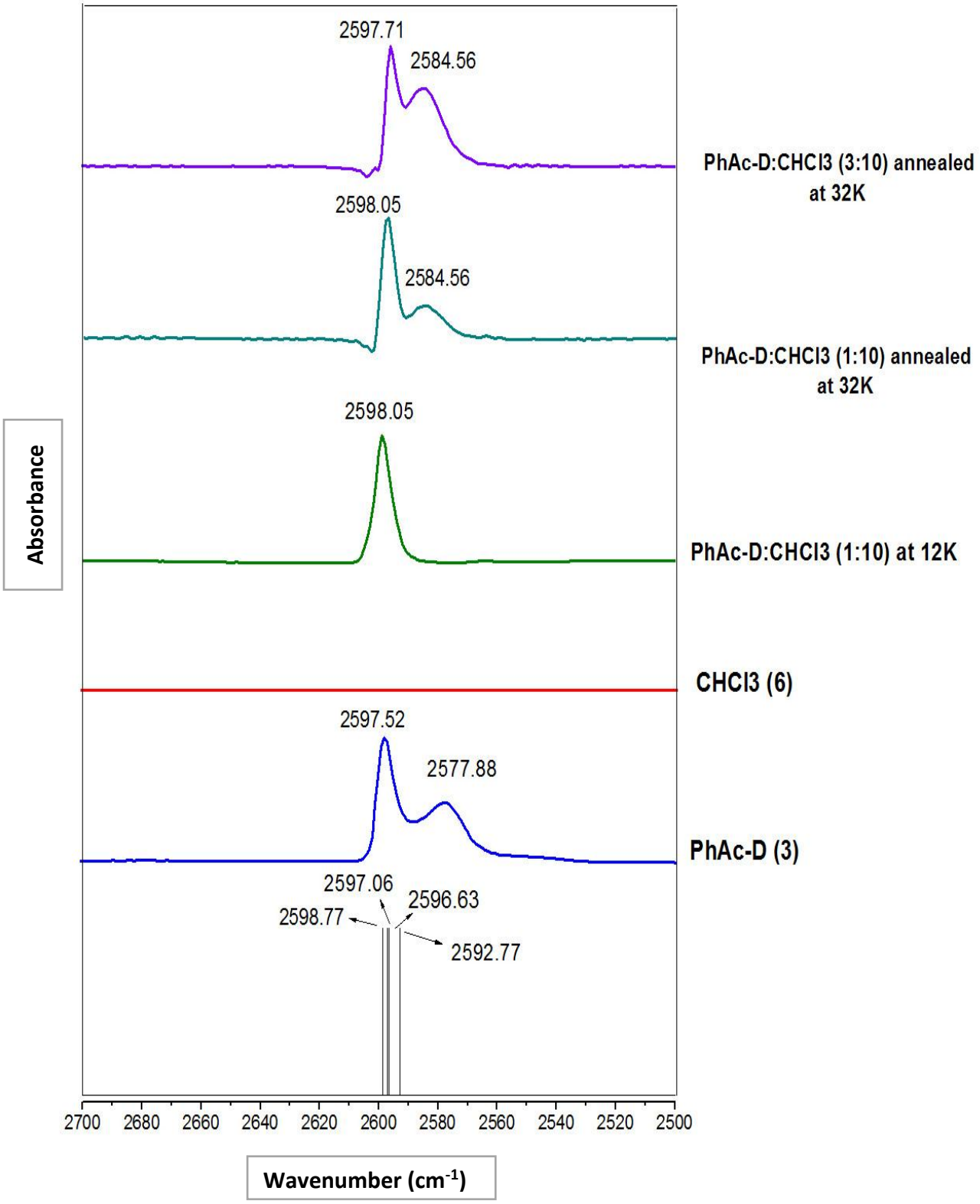

Fig 9 (a). Spectrum of PhAc-D and PhAc-D – $CHCl_3$ complexes in Nitrogen matrix and its comparison with computed frequency at B3LYP/6-311G++ (d,p)

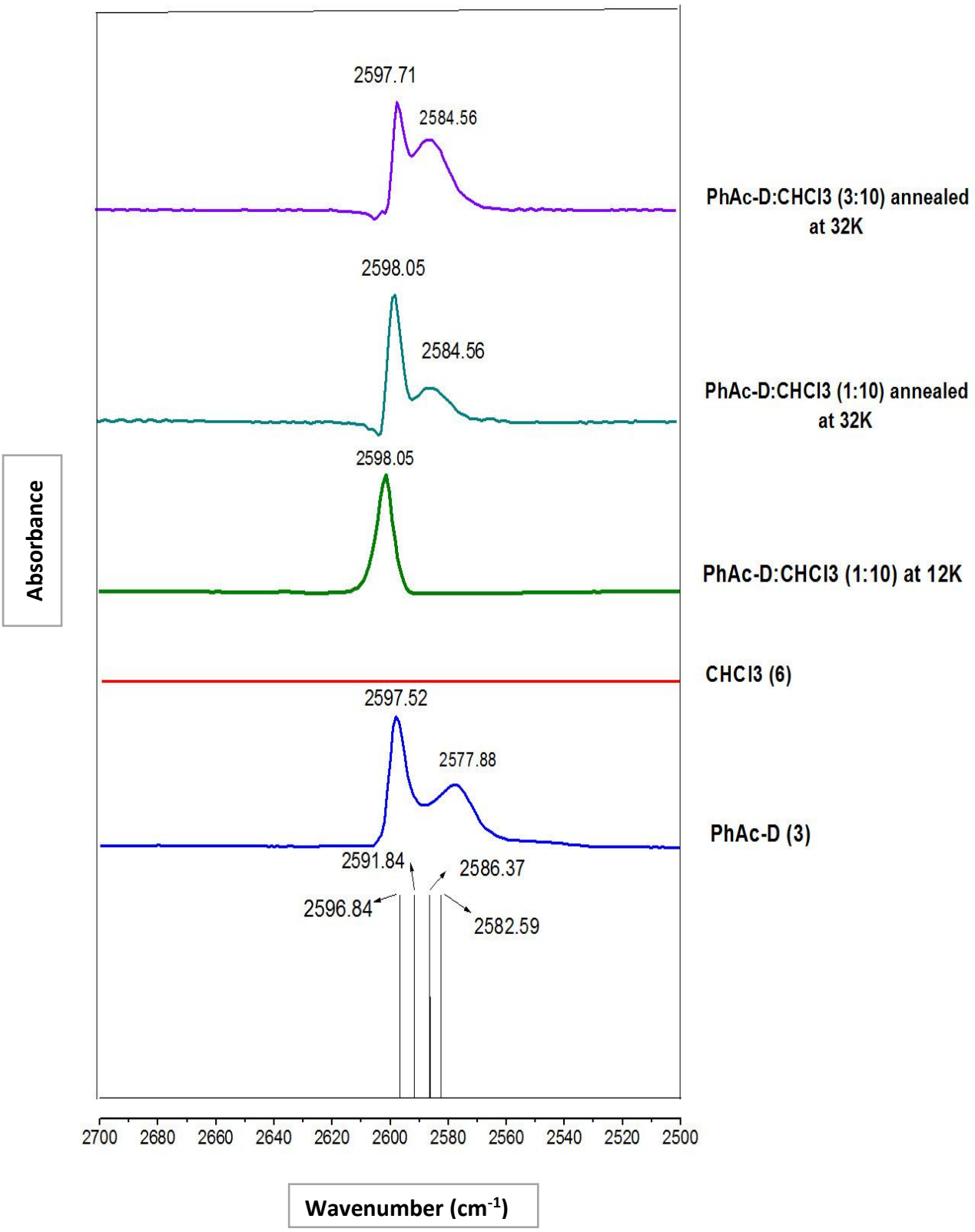

Fig 9 (b). Spectrum of PhAc-D and PhAc-D – $CHCl_3$ complexes in Nitrogen matrix and its comparison with computed frequency at M06-2X/6-311G++ (d,p)

The feature at 2595.14 cm^{-1} in **Fig 8 (a & b)** and 2584.56 cm^{-1} in **Fig 9 (a & b)** can be assigned to C-D stretching mode of the PhAc-D submolecule in the PhAc-D – $CHCl_3$ complex. The assignment indicates a redshift by 11.72 cm^{-1} in argon matrix and 13.49 cm^{-1} in nitrogen matrix in the C-D stretch of the PhAc-D sub molecule from the value obtained for free PhAc-D for this mode following complex formation.

The spectral feature of PhAc-D dimer was observed at 2575.68 cm^{-1} in the argon matrix while the same feature appeared at 2577.88 cm^{-1} in the nitrogen matrix.

Experiments with $CDCl_3$ and PhAc-D were also carried out in both the matrices. Similar spectral features were observed in the C-D stretch region of PhAc-D. This mode appeared at 2607.15 cm^{-1} in the PhAc-D alone spectra in the Argon matrix as shown in **Fig 10 (a & b)**. Upon codeposition the product feature appeared at 2595.00 cm^{-1} along with the site effect feature at 2598.70 cm^{-1}.

In nitrogen matrix, the C-D stretching mode was observed at 2598.62 cm^{-1} in PhAc-D alone spectra, while the complex peak was observed at 2584.66 cm^{-1} **(Fig 11 (a& b)).** Experiments in both the matrices showed PhAc-D dimer feature at 2575.18 cm^{-1} and 2578.67 cm^{-1} in argon and nitrogen respectively. As observed in the case of PhAc-D - $CHCl_3$ the complex feature increased in intensity as the PhAc-D and $CDCl_3$ concentrations were increased.

No other vibrational features pertaining to the complexes could be observed, probably because its intensity may have been too low to be discerned.

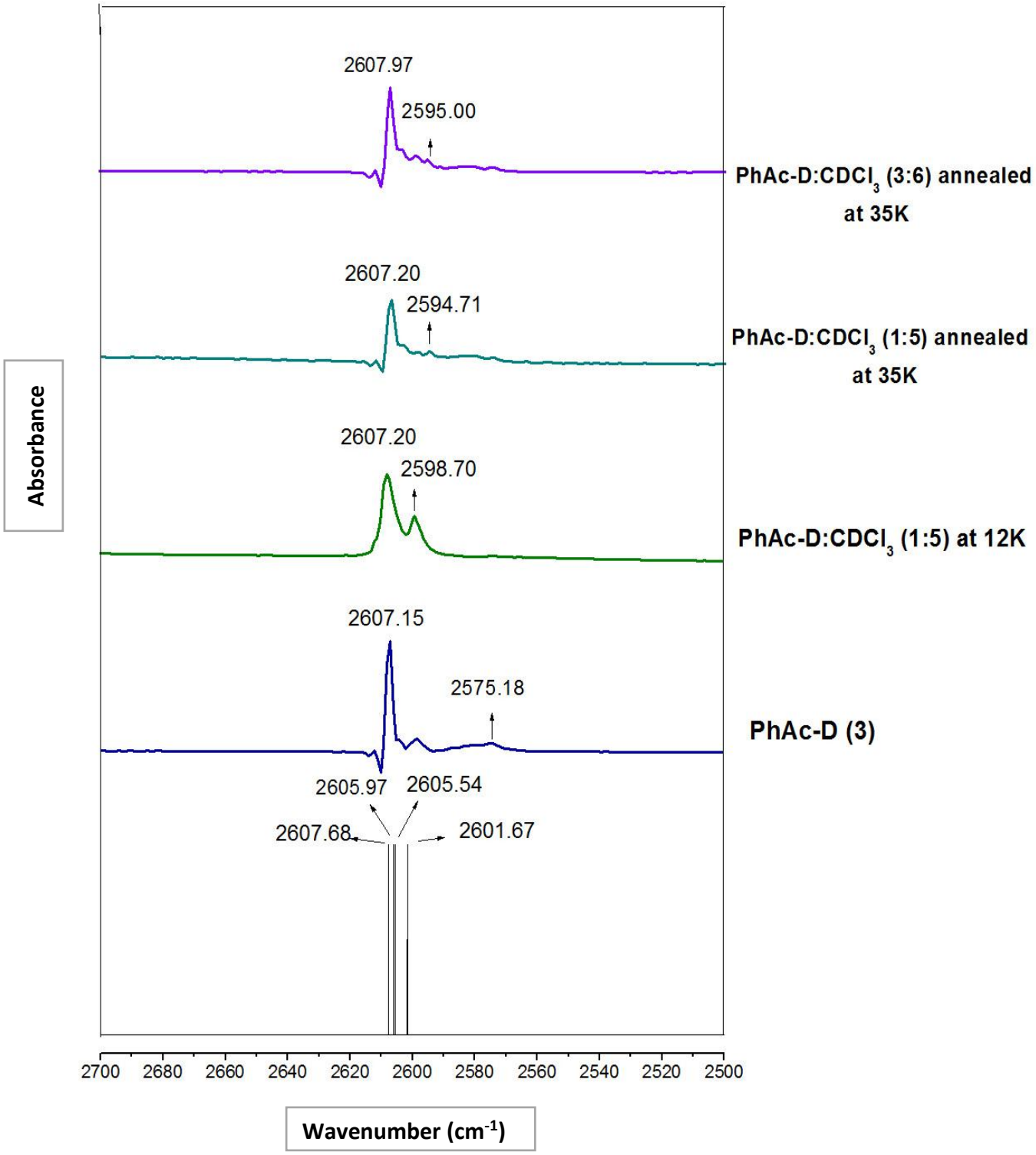

Fig 10 (a). Spectrum of PhAc-D and PhAc-D – $CDCl_3$ complexes in Argon matrix and its comparison with computed frequency at B3LYP/6-311G++ (d,p)

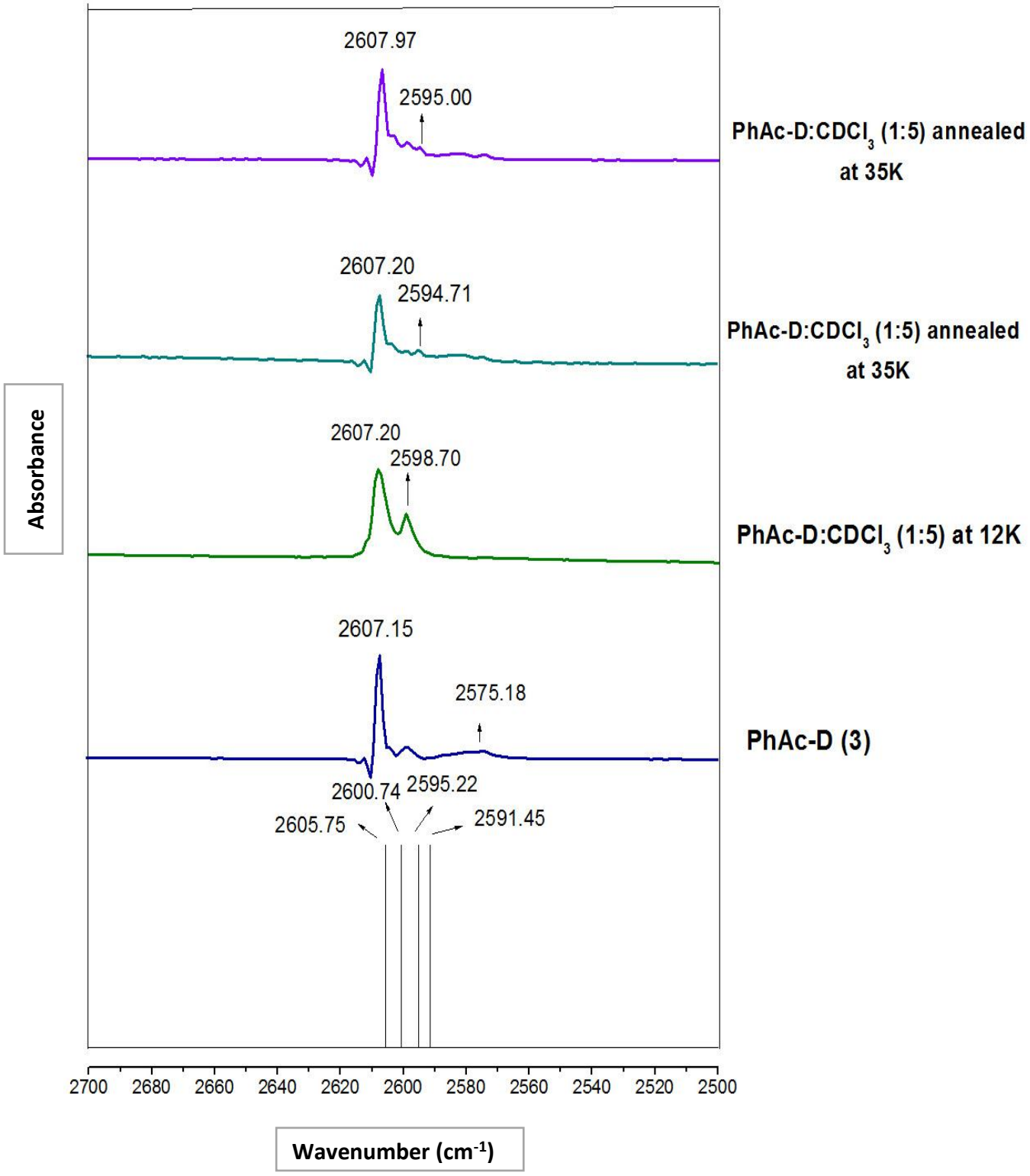

Fig 10 (b). Spectrum of PhAc-D and PhAc-D – $CDCl_3$ complexes in Argon matrix and its comparison with computed frequency at M06-2X/6-311G++ (d,p)

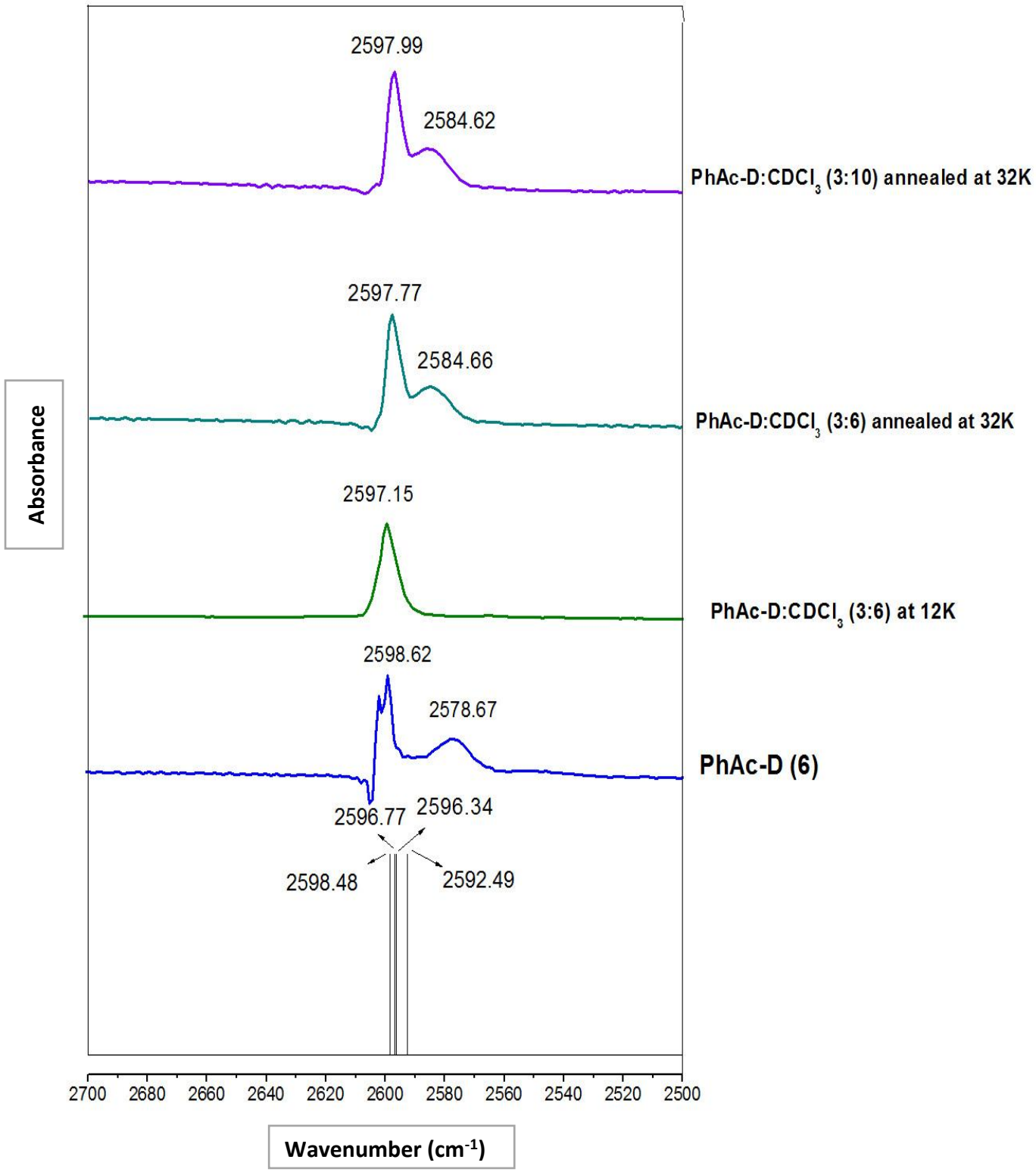

Fig 11 (a). Spectrum of PhAc-D and PhAc-D – $CDCl_3$ complexes in Nitrogen matrix and its comparison with computed frequency at B3LYP/6-311G++ (d,p)

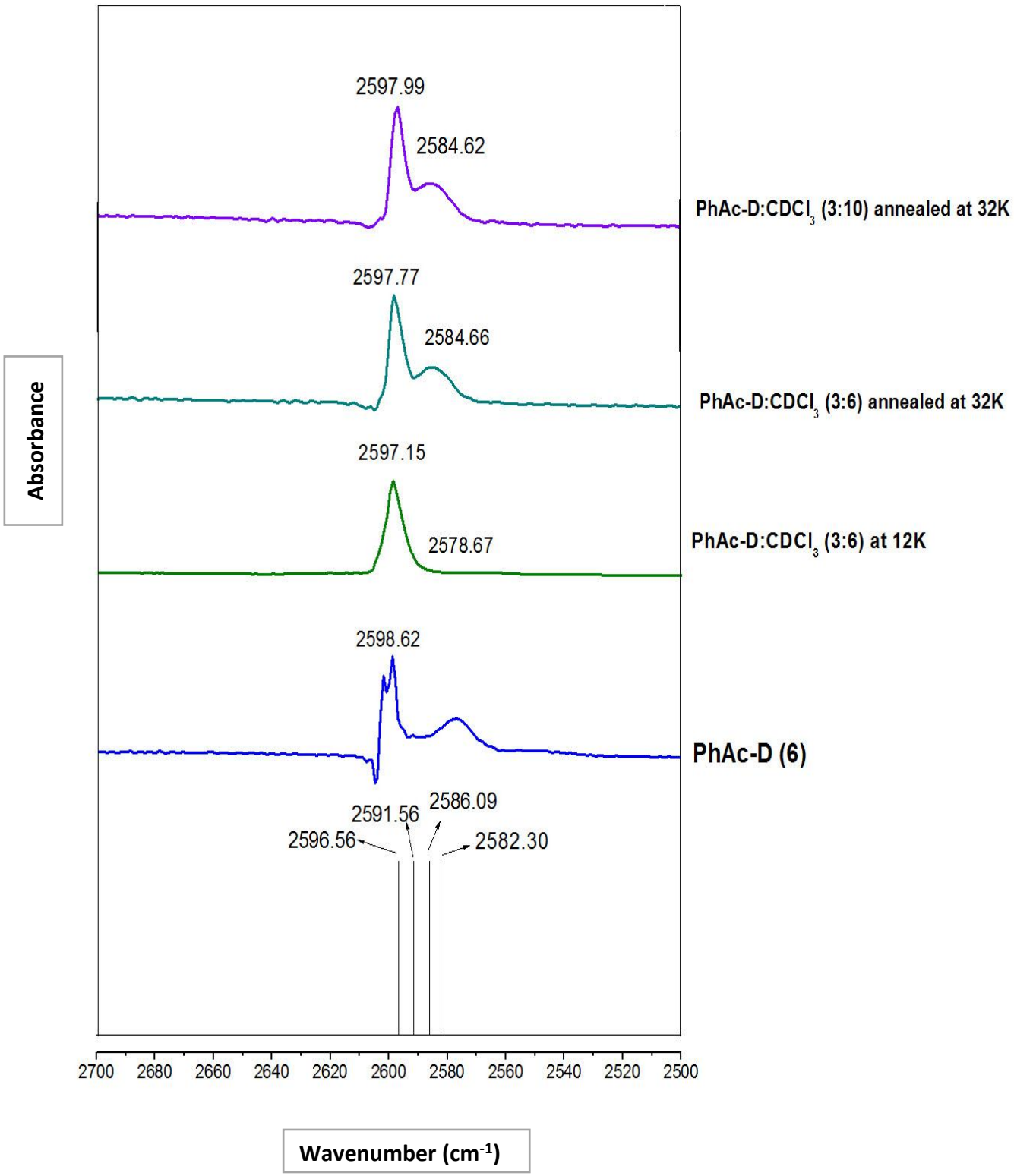

Fig 11 (b). Spectrum of PhAc-D and PhAc-D – $CDCl_3$ complexes in Nitrogen matrix and its comparison with computed frequency at M06-2X/6-311G++ (d,p)

3.2.2 Structure of the PhAc-D – $CHCl_3$ and PhAc-D - $CDCl_3$ complexes and interaction energies:

As mentioned above, computations of phenylacetylene-D – chloroform complexes were performed at M06-2X and B3LYP levels of theory using 6-311++G (d,p) basis set. Calculations showed the existence of basically four complexes which corresponded to a minimum on the potential energy surface. While three of these complexes are hydrogen bonded, the fourth is non-hydrogen bonded complex. **Fig 12 (a & b)** show the optimized structures of the complexes and their stabilization energies calculated at B3LYP and M06-2X levels of theory respectively.

Calculations show the existence of complex 1 as the global minima at B3LYP/6-311++G (d,p) level of theory. This conformer consists of the chloroform molecule present on top of the phenylacetylene molecule with the hydrogen atom pointing towards the acetylenic group. The hydrogen atom of $CHCl_3$ seems to be approaching the π-electron density of the acetylenic triple bond in a near perpendicular fashion. While one of the C-Cl bonds is aligned nearly parallel to the acetylenic C-H Bond, others have no particular alignment. The H…C1(Ac) distance is approximately 2.74 Å and H…C2(Ac) distance is approximately 2.68 Å. This distance is consistent with the typical hydrogen bond interaction in C-H…. π systems [63]. Furthermore, the C-H… π interaction of chloroform with acetylenic cloud of PhAc-D was verified with AIM calculations which showed a substantial value of electronic charge density at the bond critical point. The computed binding energies, the BSSE corrected energy, and the ZPE corrected energy calculated for complex 1 is -2.18 kcal/mol, -1.38 kcal/mol and -1.88 kcal/mol respectively.

The complex 2 has a structure where the chloroform H is interacting with the benzene-π cloud of PhAc-D molecule. The stabilization energy of complex 2 is slightly lower than complex 1 at the B3LYP/6-311++G (d,p) level. The uncorrected binding energy for complex 2 at this level is -1.74 kcal/mol and ZPE corrected and BSSE corrected energies are -1.53 kcal/mol and -0.78 kcal/mol respectively. The structure depicts the hydrogen of chloroform pointing towards the centre of the benzene- π cloud with the chloroform C-H bond in near perpendicular alignment with the π cloud. The distance between the hydrogen atom and the centre of the benzene- π cloud is 2.79 Å. The typical distance between hydrogen and π cloud is in the range of 2.5-2.9 Å, which is in good agreement with the literature [64].

Complex 1 (-2.18/-1.88/-1.38)

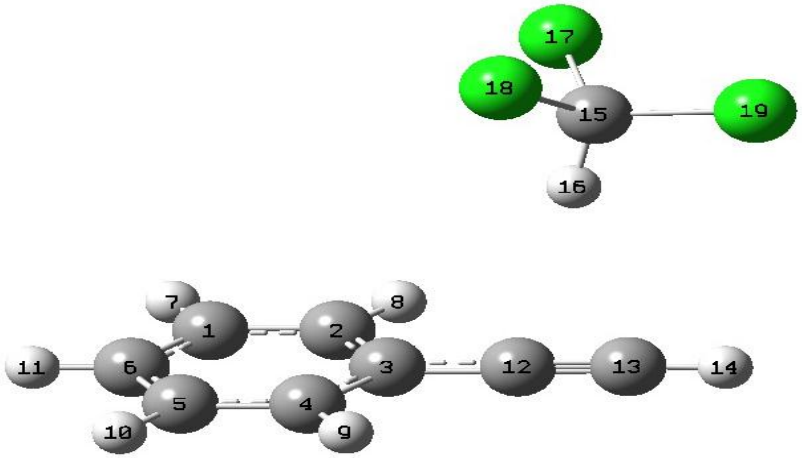

Complex 2 (-1.74/-1.53/-0.78)

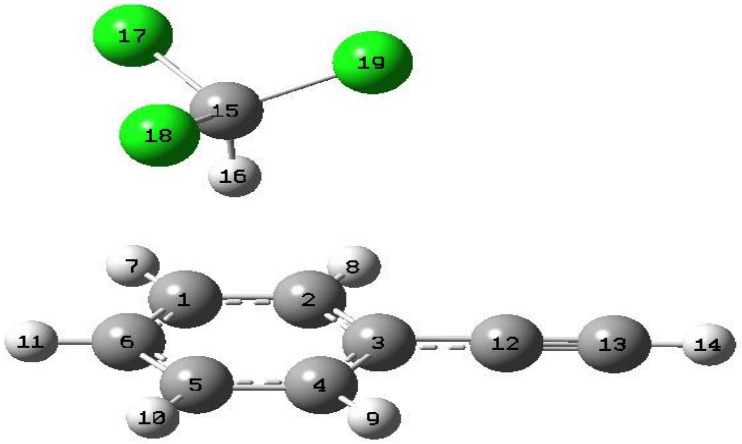

Complex 3 (-0.63/-0.42/-0.01)

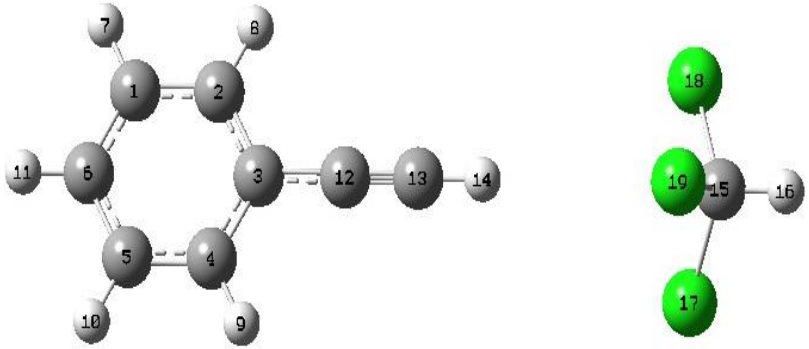

Complex 4 (-0.58/-0.41/-0.10)

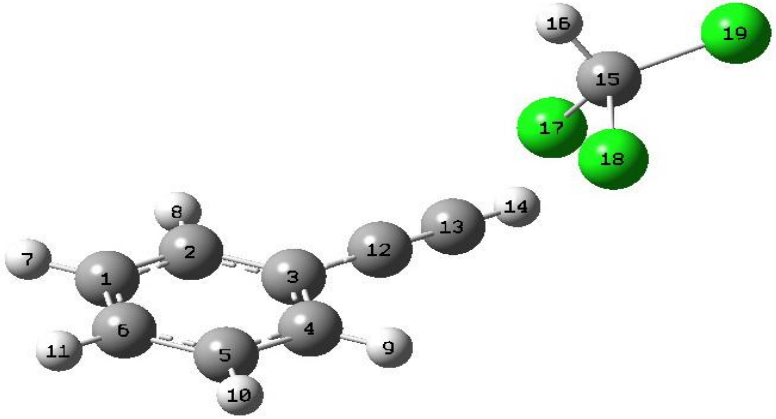

Fig 12 (a): Optimized geometry and the stabilization energies (Raw/ZPE/BSSE in kcal/mol) of complexes at B3LYP/6-311G++ (d,p)

Complex 1 (-6.57/-6.23/-5.12)

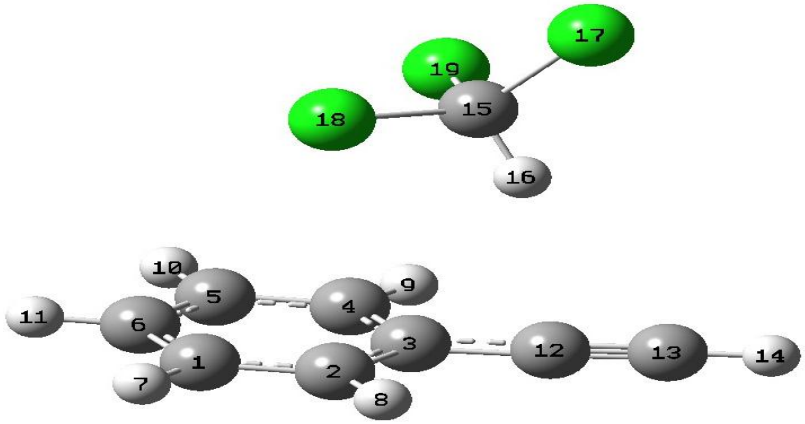

Complex 2 (-7.17/-6.62/-5.65)

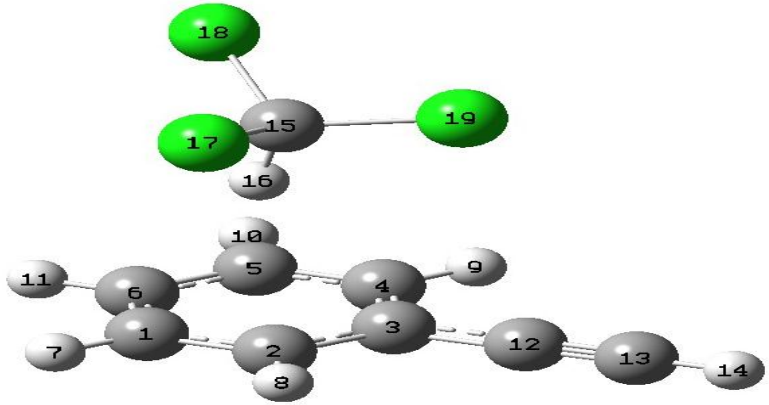

Complex 3 (-1.64/-1.49/-0.87)

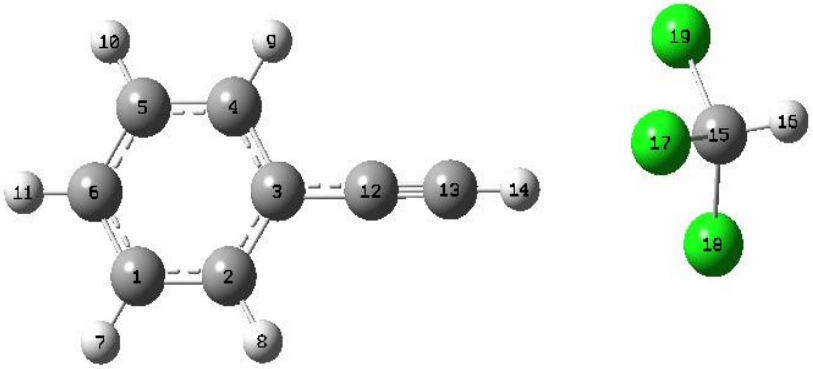

Complex 4 (-4.26/-3.99/4.26)

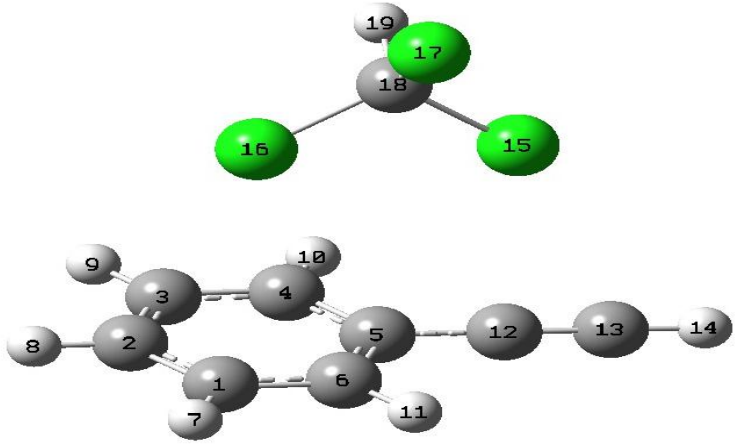

Fig 12 (b): Optimized geometry and the stabilization energies (Raw/ZPE/BSSE in kcal/mol) of complexes at M06-2X/6-311G++ (d,p)

Complex 3, on the other hand does not involve any H- π interactions. The structure shows an n-sigma interaction between the three chlorine atoms and the acetylenic hydrogen. The bond distances between the chlorine atoms and the acetylenic hydrogen lie in the range 3.7-3.9 Å classifying clearly as a weak electrostatic interaction. One might expect to see the acetylenic hydrogen to interact with the electron cloud of the three chlorine atoms centered around the chloroform carbon. But AIM calculations show otherwise.

Calculations predict complex 4 to be the lowest energy complex of all. It has a structure where the chlorine atom interacts with the acetylenic- π cloud through weak interactions. The Cl….C1(Ac) distance is 3.62 Å and the Cl….C2(Ac) distance is 3.69 Å which is in good agreement with the Cl… π distances reported in the literature [65]. AIM calculations were performed on all the complexes. The electron density, the Laplacian of electron density were computed at the critical points and the values are shown in table.

At M06-2X/6-311++G (d,p) level of theory, complex 2 is shown to be the lowest energy configuration. The energy difference between complex 1 and complex 2 is hardly significant. The orientation of atoms in complex 2 at M06-2X/6-311++G (d,p) is almost similar to that at B3LYP/6-311++G (d,p) with some minor variations. Complex 4 has a structure with one chlorine atom interacting with one of the acetylenic carbons and the other interacting with one of the benzene carbons. Stabilization energy values of complexes 3 and 4 is quite low compared to that of complexes 1 and 2. AIM study with these complexes at M06-2X/6-311++G (d,p) level showed an additional interaction of Chlorine with carbon atom with low electronic charge density values of about ~0.006 e/(bohr)^3.

3.2.3 Vibrational assignments:

The vibrational frequencies of the monomers and their complexes were calculated at B3LYP and M06-2X levels using 6-311++G (d,p) basis set. **Table 2** below shows the computed frequency values at these two levels of theory along with their shifts. **Table 3** presents the same for the PhAc-D – $CDCl_3$ complexes. The computed frequency for the C-D stretching mode was scaled by comparing its frequency for the uncomplexed PhAc-D or $CHCl_3$ with that obtained experimentally. The scaling factor thus obtained was then used to scale the computed frequency in the complex. The scaling factor for the C-D stretching mode is given in the **Table 4** (for PhAc-D – $CHCl_3$ complexes) and

PhAc-D	**Complex1**	**Δν**	**Complex2**	**Δν**	**Complex3**	**Δν**	**Complex4**	**Δν**	**Mode Assignment**
504.47	510.19	5.72	508.15	3.68	522.38	17.91	551.95	47.48	C-D Bend Out of Plane
571.11	573.11	2	573.64	2.53	582.85	11.74	571.17	0.06	C-D Bend In Plane
2058.95	2053.67	-5.28	2060.51	1.56	2058.49	-0.46	2057.52	-1.43	C≡C Stretch
2711.65	2706.14	-5.51	2712.39	0.74	2710.61	-1.04	2710.16	-1.49	C-D Stretch
CHCl3	**Complex1**	**Δν**	**Complex2**	**Δν**	**Complex3**	**Δν**	**Complex4**	**Δν**	**Mode Assignment**
3176.45	3179.87	3.42	3195.61	19.16	3193.69	17.24	3191.93	15.48	C-H Stretch
1245.28 1245.62	1267.14 1269.03	21.86 23.41	1248.07 1249.38	2.79 3.76	1248.51 1248.9	3.23 3.28	1247.41 1248.93	2.13 3.31	C-H Bend (Degenerate modes)
729.26	727.42	-1.84	727.39	-1.87	729.94	0.68	733.3	4.04	C-Cl Stretch

Table 2 (a): Calculated vibration frequency shifts (in cm^{-1}) for PhAc-D – $CHCl_3$ complexes at B3LYP/6-311++G (d,p)

PhAc-D	**Complex1**	**Δν**	**Complex2**	**Δν**	**Complex3**	**Δν**	**Complex4**	**Δν**	**Mode Assignment**
575.85	526.11	-49.74	573.81	-2.04	582.95	7.1	567.3	-8.55	C-D Bend Out of Plane
599.5	597.69	-1.81	598.3	-1.2	597.04	-2.46	598.41	-1.09	C-D Bend In Plane
2090.69	2082.65	-8.04	2093.62	2.93	2083.97	-6.72	2087.58	-3.11	C≡C Stretch
2740.01	2727.69	-12.32	2738.73	-1.28	2723.7	-16.31	2733.46	-6.55	C-D Stretch
CHCl3	**Complex1**	**Δν**	**Complex2**	**Δν**	**Complex3**	**Δν**	**Complex4**	**Δν**	**Mode Assignement**
3197.35	3233.4	36.05	3282.26	84.91	3231.65	34.3	3233.63	36.28	C-H Stretch
1265.18 1266.18	1265.29 1276.39	0.11 10.21	1258.79 1273.86	-6.39 7.68	1263.17 1264.63	-2.01 -1.55	1263.55 1268.07	-1.63 1.89	C-H Bend (Degenerate modes)
795.97	784.83	-11.14	796.04	0.07	805.93	9.96	804.27	8.3	C-Cl Stretch

Table 2 (b): Calculated vibration frequency shifts (in cm^{-1}) for PhAc-D – $CHCl_3$ complexes at M06-2X/6-311++G (d,p)

PhAc-D	**Complex1**	**Δν**	**Complex2**	**Δν**	**Complex3**	**Δν**	**Complex4**	**Δν**	**Mode Assignment**
504.47	510.17	5.7	508.15	3.68	522.38	17.91	503.35	-1.12	C-D Bend Out of Plane
571.11	573.10	1.99	573.64	2.53	582.85	11.74	571.17	0.06	C-D Bend In Plane
2058.95	2053.65	-5.3	2060.51	1.56	2058.49	-0.46	2057.52	-1.43	C≡C Stretch
2711.65	2706.15	-5.5	2712.39	0.74	2710.61	-1.04	2710.16	-1.49	C-D Stretch
CDCl3	**Complex1**	**Δν**	**Complex2**	**Δν**	**Complex3**	**Δν**	**Complex4**	**Δν**	**Mode Assignment**
2348.32	2341.02	-7.3	2351.91	3.59	2350.52	2.20	2349.17	0.85	C-D Stretch
922.75 922.90	933.98 934.91	11.23 12.01	921.73 923.53	-1.02 0.63	922.49 922.87	-0.26 -0.03	920.51 923.10	-2.24 0.2	C-D Bend (Degenerate modes)
708.47	706.24	-2.23	706.75	-1.72	710.22	1.75	712.50	4.03	C-Cl Stretch

Table 3 (a): Calculated vibration frequency shifts (in cm^{-1}) for PhAc-D – $CDCl_3$ complexes at B3LYP/6-311++G (d,p)

PhAc-D	**Complex1**	**Δν**	**Complex2**	**Δν**	**Complex3**	**Δν**	**Complex4**	**Δν**	**Mode Assignment**
575.85	569.88	-5.97	573.8	-2.05	582.85	7	567.3	-8.55	C-D Bend Out of Plane
599.5	597.69	-1.81	598.30	-1.2	597.4	-2.1	598.41	-1.09	C-D Bend In Plane
2090.69	2082.64	-8.05	2093.61	2.92	2083.86	-6.83	2087.58	-3.11	C≡C Stretch
2740.01	2727.690	-12.32	2738.73	-1.28	2723.45	-16.56	2733.46	-6.55	C-D Stretch
CDCl3	**Complex1**	**Δν**	**Complex2**	**Δν**	**Complex3**	**Δν**	**Complex4**	**Δν**	**Mode Assignement**
2359.64	2379.31	19.67	2412.14	52.5	2378.69	19.05	2379.69	20.05	C-D Stretch
945.77 947.07	944.41 950.32	-1.36 3.25	937.85 953.00	-7.92 5.93	946.39 949.42	0.62 2.35	945.31 949.09	-0.46 2.02	C-D Bend (Degenerate modes)
761.44	784.83	23.39	767.21	5.77	764.08	2.64	771.46	10.02	C-Cl Stretch

Table 3(b): Calculated vibration frequency shifts (in cm^{-1}) for PhAc-D – $CDCl_3$ complexes at M06-2X/6-311++G (d,p)

Complex	**Calculated ν (cm^{-1}) (unscaled)**	**Calculated ν (cm^{-1}) (scaled) Nitrogen**	***Computed Shift (N_2)* ν (cm^{-1})**	**Scaling Factor**	***Exp.* ν (cm^{-1})**	**Calculated ν (cm^{-1}) (scaled) Argon**	***Computed Shift (Ar)* *ν (cm^{-1})***	**Scaling Factor**	***Exp.* ν (cm^{-1})**
PhAc-D	2711.65	2598.05	-	0.9581	2598.05	2607.87	-	0.9614	2607.87
Complex 1	2706.14	2592.77	5.28	0.9581	2584.56	2601.57	6.3	0.9614	2595.05
Complex 2	2712.39	2598.77	-0.72	0.9581	2584.56	2607.58	0.29	0.9614	2595.05
Complex 3	2710.61	2597.06	0.99	0.9581	2584.56	2605.87	2	0.9614	2595.05
Complex 4	2710.16	2596.63	1.42	0.9581	2584.56	2605.44	2.43	0.9614	2595.05

Table 4 (a): Experimental and Computed frequencies along with their scaling factors at B3LYP/6-311++G (d,p) for the PhAc-D – $CHCl_3$ adduct

Complex	**Calculated ν (cm^{-1}) (unscaled)**	**Calculated ν (cm^{-1}) (scaled) Nitrogen**	***Computed Shift (N_2)* ν (cm^{-1})**	**Scaling Factor**	***Exp.* ν (cm^{-1})**	**Calculated ν (cm^{-1}) (scaled) Argon**	***Computed Shift (Ar)* *ν (cm^{-1})***	**Scaling Factor**	***Exp.* ν (cm^{-1})**
PhAc-D	2740.01	2598.05	-	0.9482	2598.05	2607.87	-	0.9514	2607.87
Complex 1	2727.69	2586.32	11.73	0.9482	2584.56	2595.15	12.72	0.9514	2595.05
Complex 2	2738.73	2596.84	1.21	0.9482	2584.56	2605.66	2.21	0.9514	2595.05
Complex 3	2723.7	2582.59	15.46	0.9482	2584.56	2591.36	16.51	0.9514	2595.05
Complex 4	2733.46	2591.84	6.21	0.9482	2584.56	2600.64	7.23	0.9514	2595.05

Table 4 (b): Experimental and Computed frequencies along with their scaling factors at M06-2X/6-311++G (d,p) for the PhAc-D – $CHCl_3$ adduct

Complex	**Calculated ν (cm^{-1}) (unscaled)**	**Calculated ν (cm^{-1}) (scaled) Nitrogen**	***Computed Shift (N_2)* ν (cm^{-1})**	**Scaling Factor**	***Exp.* ν (cm^{-1})**	**Calculated ν (cm^{-1}) (scaled) Argon**	***Computed Shift (Ar) ν (cm^{-1})***	**Scaling Factor**	***Exp.* ν (cm^{-1})**
PhAc-D	2711.65	2597.77	-	0.958	2597.77	2607.97	-	0.9614	2607.97
Complex 1	2706.14	2592.49	5.28	0.958	2584.66	2601.67	6.30	0.9614	2595.00
Complex 2	2712.39	2598.48	-0.71	0.958	2584.66	2607.68	0.29	0.9614	2595.00
Complex 3	2710.61	2597.77	0.0	0.958	2584.66	2605.95	2.02	0.9614	2595.00
Complex 4	2710.16	2596.34	1.43	0.958	2584.66	2605.54	2.43	0.9614	2595.00

Table 5 (a): Experimental and Computed frequencies along with their scaling factors at B3LYP/6-311++G (d,p) for the PhAc-D – $CDCl_3$ adduct

Complex	**Calculated ν (cm^{-1}) (unscaled)**	**Calculated ν (cm^{-1}) (scaled) Nitrogen**	***Computed Shift (N_2)* ν (cm^{-1})**	**Scaling Factor**	***Exp.* ν (cm^{-1})**	**Calculated ν (cm^{-1}) (scaled) Argon**	***Computed Shift (Ar) ν (cm^{-1})***	**Scaling Factor**	***Exp.* ν (cm^{-1})**
PhAc-D	2740.01	2597.77	-	0.948	2597.77	2607.97	-	0.9514	2607.97
Complex 1	2727.69	2586.09	11.68	0.948	2584.66	2595.22	12.75	0.9514	2595.00
Complex 2	2738.73	2596.56	1.21	0.948	2584.66	2605.75	2.22	0.9514	2595.00
Complex 3	2723.7	2582.30	15.47	0.948	2584.66	2591.45	16.52	0.9514	2595.00
Complex 4	2733.46	2591.56	6.21	0.948	2584.66	2600.74	7.23	0.9514	2595.00

Table 5 (b): Experimental and Computed frequencies along with their scaling factors at M06-2X/6-311++G (d,p) for the PhAc-D – $CDCl_3$ adduct

Table 5 (for PhAc-D – $CDCl_3$ complexes). It is important to note that complexes 1 and 2 are almost equal in energy with B3LYP favouring the former and M06-2X favouring the later. The probability of their formation is more than with complexes 3 and 4. Hence, the shifts resulting from the complexes 1 and 2 is more likely to be prominent.

As mentioned earlier, the C-D stretch of the PhAc-D sub molecule in the PhAc-D – $CHCl_3$ complex is observed at 2595.14 cm^{-1} in argon matrix. This value agrees well with the scaled computed value of 2595.15 cm^{-1} for this mode in the complex at M06-2X level of theory. This mode in the complex at B3LYP is at 2601.57 cm^{-1}. In nitrogen matrix, the same mode is observed experimentally in the complex at 2584.56 cm^{-1}, which is in good agreement with the scaled computed value of 2580.32 cm^{-1} in the complex at M06-2X level. The mode in the complex at B3LYP is at 2592.77 cm^{-1}.

In the PhAc-D – $CDCl_3$ complex, the C-D stretch of the PhAc-D sub molecule appears at 2595.00 cm^{-1} which agrees well with the scaled computed value of 2595.22 cm^{-1} for this mode in the complex at M06-2X level. B3LYP calculates this mode to be at 2601.67 cm^{-1}. In nitrogen matrix, the complex feature observed at 2584.66 cm^{-1} also agrees well with the scaled computed value in the complex at 2586.09 cm^{-1} at M06-2X. The mode in the complex at B3LYP is calculated at 2592.49 cm^{-1}

The computationally derived complex 1, which is of the H-π type complex, with PhAc-D being the proton acceptor agrees well with the experimental results in both PhAc-D – $CHCl_3$ and PhAc-D –$CDCl_3$ experiments. Further, the experimental shifts observed in the C-D stretch of PhAc-D sub molecule in the complexes also support the computationally predicted structure of the complex. The small shift (~12 cm^{-1}) in this mode of the PhAc-D sub molecule in the complex as opposed to larger shifts as observed in acetylene-water complex [66], indicate that PhAc-D acts as a proton acceptor in the complex.

3.3 AIM analysis:

An analysis of the charge density topology was performed using Atoms in Molecules (AIM 2000) theory proposed by Bader. The (3,-1) critical points were located for all the complexes. The electron density $\rho(r)$ and Laplacian of electron density $\nabla^2\rho(r)$ were computed for these critical points for which the values are shown in the **Table 6 & 7**. The $\rho(r)$ and $\nabla^2\rho(r)$ values for bond critical points in the complexes were found to be of the order of 10^{-3} au. **Fig 13 & 14** show the AIM calculated geometry for the complexes at both B3LYP and M06-2X levels of theory respectively. The red points between two atoms represent the (3,-1) critical point. The larger the electron density for a critical point, the higher is the strength of the non covalent interaction.

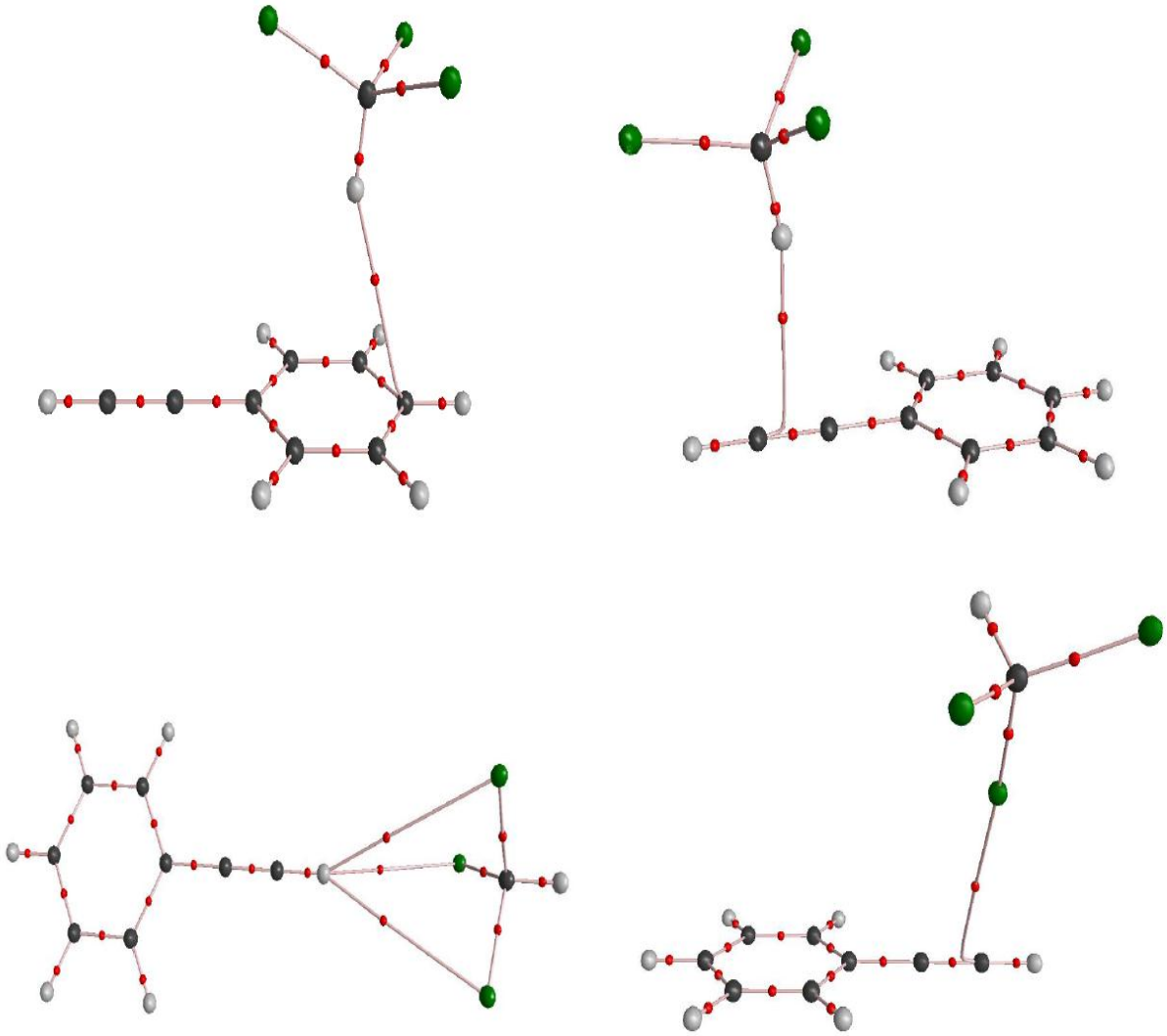

Figure 13: Structures of complexes showing the bond critical points at B3LYP/6-311++G (d,p)

Complex	ρ (r) e/(bohr)^3	$\nabla^2\rho$(r) e/(bohr)^5
Complex 1	0.00829	-0.00550
Complex 2	0.00496	-0.00351
Complex 3	0.00091, 0.00099, 0.00104	-0.00079, -0.00084, -0.00087
Complex 4	0.00421	-0.00341

Table 6: AIM calculation of the complexes at B3LYP/6-311++G (d,p)

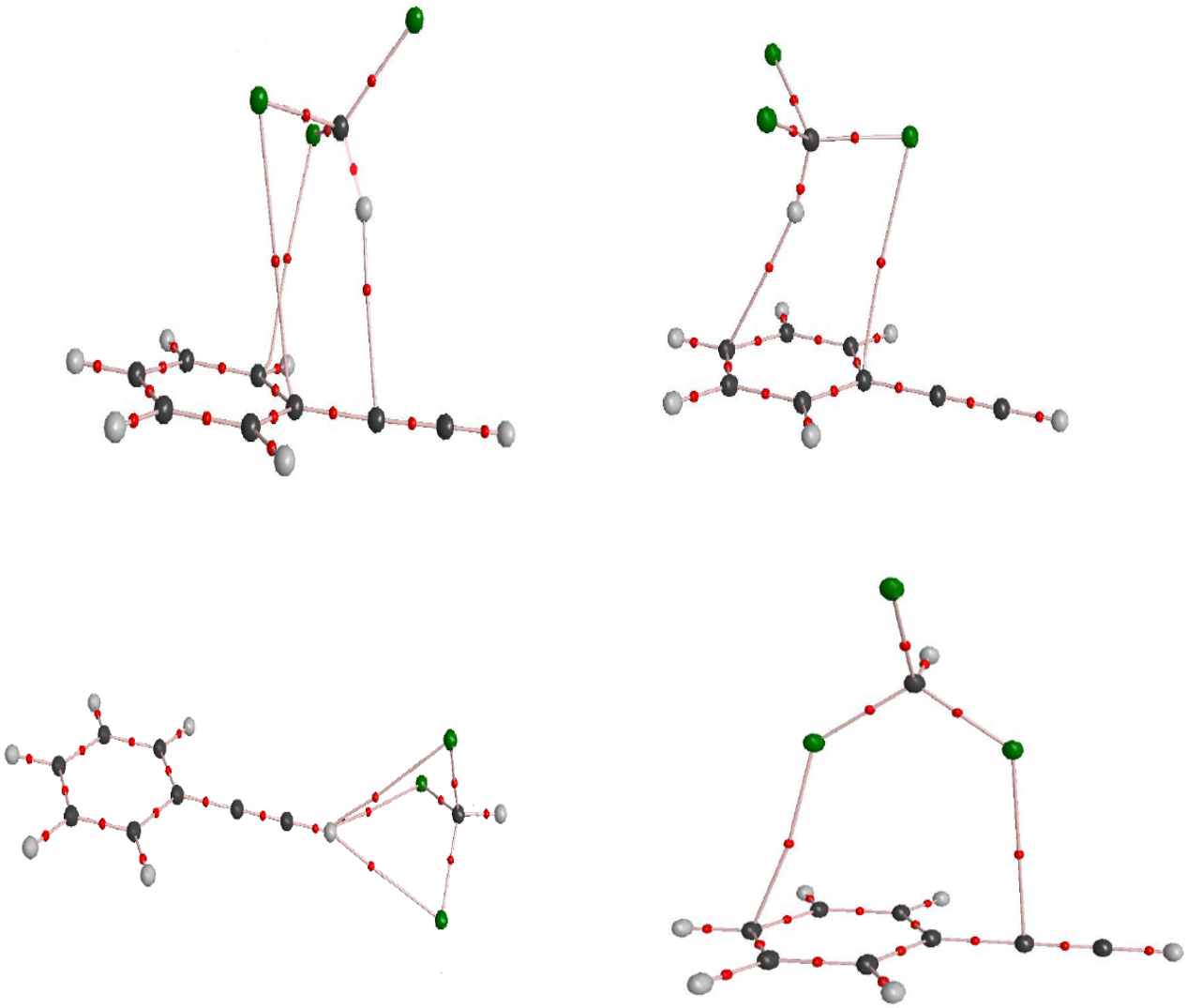

Figure 14: Structures of complexes showing the bond critical points at M06-2X/6-311++G (d,p)

Complex	ρ (r) e/(bohr)^3	$\nabla^2\rho$(r) e/(bohr)^5
Complex 1	0.00918, 0.00603, 0.00564	-0.00732, -0.00466, -0.00449
Complex 2	0.00918, 0.00613	-0.00761, 0.00481
Complex 3	0.00335, 0.00332, 0.00447	-0.00262, -0.00262, -0.00339
Complex 4	0.00705, 0.00662	-0.006111, -0.00553

Table 7: AIM calculation of the complexes at M06-2X/6-311++G (d,p)

3.4 Geometrical parameters:

Major parameters indicative of a bond formation are the bond lengths and bond angles. These along with other bond parameters aid in explaining the magnitude in frequency shift. Albeit miniscule, upon complexation there is often some changes in bond parameters of the individual molecules. These changes show how strong or weak the interaction is between the monomers. Some of the important bond parameters were calculated at B3LYP and M06-2X levels of theory. **Table 8 (a,b,c,d)** below shows the important structural parameters calculated for all the four complexes at both the levels.

Complex parameter	B3LYP	M06-2X
C15-Cl19	1.79	1.77
C12-H16	2.74	2.52
C13-H16	2.68	2.94
C15-H16	1.08	1.08
C13-H14	1.06	1.06
C12-C13	1.21	1.20
H14-Cl19	3.83	-
H14-C13-H16	100.98	122.75
C3-C12-H16	105.49	79.92
H16-C15-Cl19	107.27	-
H16-C15-Cl18	-	108.12
C13-H14-Cl17	-	101.37
C13-H14-Cl19	96.99	-
C2-C3-C12-H16	81.66	-105.54
Cl19-C15-H16-C13	-8.21	-
Cl17-C15-H16-C13	-	-28.04
H14-C13-C12-H16	-176.79	-173.18

Table 8 (a): Structural parameters, Bond lengths (Å), Bond angles ( ), and dihedral angles ( ) of complex 1 (as indicated in Figure 12(a) and 12(b))

Complex Parameter	B3LYP	M06-2X
C15-H16	1.08	1.08
H16-C6	2.94	2.61
C3-H16	3.22	2.66
C15-Cl18	1.79	1.77
C12-C13	1.20	1.20
C6-H16-C15	151.23	163.94
C3-H16-C15	154.82	131.85
H16-C15-Cl18	107.58	107.53
H11-C6-H16-C15	-0.30	8.45
Cl18-C15-H16-C6	62.94	-42.84
Cl18-C15-C5-H10	2.15	20.42

Table 8 (b): Structural parameters, Bond lengths (Å), Bond angles ( ), and dihedral angles ( ) of complex 2 (as indicated in Figure 12(a) and 12(b))

Complex parameter	B3LYP	M06-2X
H14-Cl18	3.76	3.02
H14-Cl19	3.84	3.23
H14-Cl17	3.79	3.22
C15-H14	3.93	3.21
C12-C13	1.20	1.20
C13-H14	1.06	1.06
C15-H16	1.08	1.08
C15-Cl17	1.79	1.77
H14-Cl19-C15	79.63	73.62
H14-Cl18-C15	81.99	79.59
H14-Cl17-C15	81.10	73.84
H14-C15-H16	178.48	175.33
H16-C15-Cl19	107.57	108.04
C13-H14-C15-H16	144.99	-176.20
C13-H14-C15-Cl19	-56.76	-52.94

Table 8 (c): Structural parameters, Bond lengths (Å), Bond angles ( ), and dihedral angles ( ) of complex 3 (as indicated in Figure 12(a) and 12(b))

Complex parameter	B3LYP	M06-2X
C13-H14	1.06	1.06
C12-C13	1.20	1.20
C15-Cl17	1.78	1.77
C15-Cl18	1.79	1.77
C15-H16	1.08	1.08
C13-C12-Cl17	76.82	95.64
H14-C13-Cl17	95.92	115.01
Cl18-C15-Cl17	111.44	110.76
H16-C15-Cl17	107.78	107.97
C3-C12-Cl17-C15	4.42	-
C5-C12-Cl17-C15	-	-11.07
H14-C13-Cl17-C15	-19.59	164.22
H14-C13-C15-Cl19	-3.42	-61.55

Table 8 (d): Structural parameters, Bond lengths (Å), Bond angles ( ), and dihedral angles ( ) of complex 4 (as indicated in Figure)

CHAPTER 4

Summary and Conclusions

4.1 Conclusion

The thesis provides a computational and experimental studies of weak interactions between formic acid and phenylacetylene-D. The experimental study has been carried out using Matrix Isolation Infrared Spectroscopy whereas the computational study has been performed by GAUSSIAN 09 [37] suite of programmes. The second section of the thesis provides a detailed knowledge about the experimental technique and its working principles. The computational analysis has been done at B3LYP and M06-2X levels of theory using a 6-311++G (d,p) basis set. The computational studies predict the formation of four different complexes between the two monomers. The structures of the complexes are similar in both the levels of theory. Complexes 1, 2 and 3 involve hydrogen bonding interactions whereas complex 4 has a non hydrogen bonding interaction between the monomers. At B3LYP, complex 1 (the hydrogen of $CHCl_3$ interacting with the acetylenic-π cloud of PhAc-D) is predicted to be the most stable structure with BSSE corrected stabilization energy as 1.38 kcal/mol. On the other hand, M06-2X anticipates complex 2 (the hydrogen of $CHCl_3$ interacting with the benzene-π cloud of PhAc-D) as the most stable structure with BSSE corrected stabilization energy as 5.65 kcal/mol. Experimental studies performed on the two monomers showed a red shift in the C-D stretching mode of PhAc-D of 11.72 cm^{-1} in argon matrix and 13.49 cm^{-1} in nitrogen matrix. The shifted peak is a possible result of the 1:1 complexation of the monomers since low concentrations of analyte was used. The vibrational frequency calculations revealed the modes C-H bend of $CHCl_3$, C-D stretch of PhAc-D and C-H stretch of $CHCl_3$ to be the highly perturbed modes of all. The calculations show shift of 5.51 cm^{-1} in the C-D stretching mode of PhAc-D at B3LYP and a shift of 12.72 cm^{-1} at M06-2X for complex 1. Other complexes hardly show any shift in this frequency mode. The experimental shift observed in this C-D stretch is in close agreement with the

computations at M06-2X level of theory thereby predicting the formation of the most stable complex 1.

We have experimentally observed and computationally proved the existence of a C-H…π complex between PhAc-D and $CHCl_3$ where PhAc-D acts a proton acceptor. "*The good agreement between computed and experimental frequencies in the complexes lends credence for the structure predicted by ab inito MO and hybrid density functional calculations*" [25].

4.2 Future outlook:

The work described in this thesis pertains to the study of weak hydrogen bonding interactions in phenylacetylene-D and chloroform. The results presented here need to be corroborated at other higher levels of theory so as to make a conclusive comment about the stable complex formation. At higher theories of computation, existence of a secondary stabilizing interaction could also be evidenced which need to be investigated. Existence of such weaker interactions may serve as a case study for investigating such possibilities in super molecules in future investigations [25].

Bibliography

1. Anslyn, Eric (2004). Modern Physical Organic Chemistry. Sausalito, CA: University Science
2. Noncovalent bonds – Molecular Cell Biology (textbook), Lodish, Berk, Zipursky, Matsudaira, Baltimore, Darnell.
3. "Lattice Energies". Retrieved 2014-01-21
4. IUPAC, Compendium of Chemical Terminology, 2nd ed. (the "Gold Book") (1997). Online corrected version: (1994) "van der Waals forces
5. Interfaces and the driving force of hydrophobic assembly, *Nature* 2005 Volume 437, Issue 7059, pp. 640-647
6. Anslyn, E.V.; Dougherty, D.A. Modern Physical Organic Chemistry; University Science Books; Sausalito, CA, 2005
7. G.Fogarasi and P.Pulay (1985) in 'Ab initio Calculation of Force Fields and Vibrational Spectra', J.Durig (ed.), Vibrational Spectra and Structure , Vol.14, Elsevier Science, Amsterdam, p.125
8. Coleman, M. M.; Graf, J. F.; Painter, P. C., Specific Interactions and the Miscibility of Polymer Blends. Technomic: Lancaster, PA, 1991.
9. "A brief history of the hydrogen bonding", Douglas A.Smith, May 5 1994, ACS
10. Latimer and Rodebush, *J. Am. Chem. Soc.*1920, 42, pp.1419.
11. Pauling, L. "the nature of the chemical bond and the structure of molecules and crystals: an introduction to modern structural chemistry", 3rd ed., Cornell Univeristy press, Ithaca, NY 1960, pp.449-504
12. Pimentel, G. C. and McClellan, A. L. "The Hydrogen Bond" W. H. Freeman and Co., San Fransisco, 1960
13. Lennard-Jones, J.; Pople, *J. A. Proc. Roy. Soc.* (London) , 205A, 155 (1951)
14. Umeyama, H.; Morokuma, K. *J. Am. Chem. Soc.* 1977, 99, 1316.

15. Arunan, E; Desiraju, G.R; Klein, R, A; Sadlej,J ; Scheiner,S; Alkorta, I; Clary, D.C; Crabtree,R.H; Dannenberg, J.J; Hobza, p; Kjaergaard, H.G; Legon, A.C; Mennucci, B; Nesbitt;D. *J. Pure Appl. Chem*. 2011, 83, 1619
16. E.R. Lippincott and R. Schroder, *J. Chem. Phys. 1955,* 23, 1099
17. L. Sobczyk, *Mol. Phys. Rep.* 1996, 14,19
18. Y. Guissani and H. Ratajczak, *Chem.Phys.* 1981, 62, 319
19. Springer,"Hydrogen Bonding: New insights", Chapter 1, R. Parthasarathi and V. Subramanian
20. Cleeland WW, Frey PA, Gerlt JA. The Low-Barrier Hydrogen Bonds in Enzymatic Catalysis (Minireview). *J Biol Chem* 1998,273, 25529-25532
21. Scheiner, S.; Hydrogen bonding. A theoretical perspective. Oxford University press, Oxford. 1997, [4,21,27,80,171]
22. Jeng, M. H.; Delaat, A. M.; Ault, B. S. *J. Phys. Chem.* 1989, 93, 3997
23. Delaat, A. M.; Ault, B. S. *J. Am. Chem. Soc.* 1987, 109, 4232
24. Hartmann, M; Wetmore, S. D.; Radom, L. *J. Phys. Chem. A.* 2001, 101, 4470.
25. E.D Jemmis, K.T Giju, K. Sundararajan, K. Sankaran, V. Vidya, K.S. Viswanathan, J. Leszczynski; *J.Mol. Struc.* 1999, 510, 59-68
26. L. George, K. Sankaran, K.S Viswanathan, C.K. Mathews, *Appl. Spectrosc*. 1994, 48, 587
27. Fumiyuki Ito, *J. Chem. Phys*. 2012,137, 014505
28. Singh, P. C.; Bandyopadhyay, B; Patwari, G. N. *J. Phys. Chem. A* 2008, 112, 3360
29. Maity, S; Guin, M; Singh, P. C; Patwari, G.N. *Chem. Phys. Chem*. 2011, 12, 26-46
30. *http://webbook.nist.gov/chemistry*
31. Maity, S; Patwari, G.N; Sedlak, R; Hobzq, P. *Phys. Chem. Chem. Phys.* 2011, 13, 16706
32. Whittle, E; Dows, D. A; Pimentel, G. C. *J. Chem. Phys.* 1954, 22, 1943
33. Hallam, H. E. Vibrational Spectroscopy of Trapped Species (Wiley Inter science Publication, London, 1973)
34. Buckingham, A. D. *Proc. Roy. Soc. (London) A* 1958, 248, 169
35. Pimentel, G. C; Charles, S. W. *Pure and Appl. Chem*. 1963, 7, 111
36. Cradock, S.; Hinchcliffe, A. J. Matrix Isolation, Chap. 2, Cambridge University Press, London (1975).

37. Gaussian 09, Revision A.1, Frisch, M. J.; Trucks, G. W.; Schlegel, H. B.; Scuseria, G. E.; Robb, M. A.; Cheeseman, J. R.; Scalmani, G.; Barone, V.; Mennucci, B.; Petersson, G. A.; Nakatsuji, H.; Caricato, M.; Li, X.; Hratchian, H. P.; Izmaylov, A. F.; Bloino, J.; Zheng, G.; Sonnenberg, J. L.; Hada, M.; Ehara, M.; Toyota, K.; Fukuda, R.; Hasegawa, J.; Ishida, M.; Nakajima, T.; Honda, Y.; Kitao, O.; Nakai, H.; Vreven, T.; Montgomery, Jr., J. A.; Peralta, J. E.; Ogliaro, F.; Bearpark, M.; Heyd, J. J.; Brothers, E.; Kudin, K. N.; Staroverov, V. N.; Kobayashi, R.; Normand, J.; Raghavachari, K.; Rendell, A.; Burant, J. C.; Iyengar, S. S.; Tomasi, J.; Cossi, M.; Rega, N.; Millam, J. M.; Klene, M.; Knox, J. E.; Cross, J. B.; Bakken, V.; Adamo, C.; Jaramillo, J.; Gomperts, R.; Stratmann, R. E.; Yazyev, O.; Austin, A. J.; Cammi, R.; Pomelli, C.; Ochterski, J. W.; Martin, R. L.; Morokuma, K.; Zakrzewski, V. G.; Voth, G. A.; Salvador, P.; Dannenberg, J. J.; Dapprich, S.; Daniels, A. D.; Farkas, Ö.; Foresman, J. B.; Ortiz, J. V.; Cioslowski, J.; Fox, D. J. Gaussian, Inc., Wallingford CT, 2009.
38. F. Biegle-Koning, R. F. W. Bader, W. -H. Tang, *J. Comput. Chem*. 2000, 96, 6796, AIM 2000
39. E. Lewars, Computational Chemistry: Introduction to theory and applications of Molecular and Quantum Mechanics, Kluwer Academic Publishers, Boston, 2003.
40. W. J. Hehre, L. Radom, P. V. R.; Schleyer J. Pople, A ab initio molecular orbital theory, John Wiley and Sons, New York, 1985.
41. J. B. Foresman, A. Frisch, Exploring chemistry with electronic structure methods, Gaussian Inc., Pittsburgh, 1993.
42. T. A. Clark, Handbook of Computational Chemistry: A practical guide to Chemical Structure and Energy Calculations, John Wiley & sons, New York, 1985.
43. D. B. Cook, Ab initio valence calculations in chemistry, Butterwort, London, 1974.
44. J. P. Lowe, Quantum Chemistry, Academic Press, New York, 1978.
45. F. Jensen, Introduction to Computational Chemistry, Wiley Publication, Second edition, 2008.
46. A. D. Becke, *Phys. Rev. A*, 1989, 38, 3098.
47. A. D. Becke, *J. Chem. Phys.*, 1983, 98, 5648.
48. C. Lee, N. Yang, R. G. Parr, *Phys. Rev. B*, 1988, 37, 785.
49. Scuseria, G. E.; Staroverov, V. N. Theory and Application of Computational

Chemistry: the first fourty years. Elsevier, 669-724

50. Zhao, Y.; Truhlar, D. G. *Theor Chem Account* 2008, 120, 215-241
51. Boys, S. F.; Bernadi, F.*; Mol. Phys*. 1970 , 19, 553
52. L. H. Jones, B. I. Swanson, *J. Chem. Phys*., 1981, 74, 3216.
53. M. Dubs, H. H. Gunthard, *Chem. Phys. Lett*., 1979, 64, 105.
54. M. Poliakoff, J. J. turner, "Infrared laser photochemistry in matrixes" in "chemical and biological application of lasers", Ed. C. B. Moore, Academic Press, New York, 1980.
55. K. Sundararajan, K. S. Viswanathan, *J. Mol. Struct.*, 2006, 798, 109.
56. K. V. J. Jose, S. R. Gadre, K. Sundararajan, K. S. Viswanathan, *J. Chem. Phys.*, 2007, 127, 104501.
57. Chapter 8, Steven W. Van Sciver, Helium Cryogenics, Springer, second edition
58. A. Oskam and D.J Stufkens, Laboratory Methods in Vibrational spectroscopy (Chap. 13), Ed H.A. Willis, J.H. Van Der maas and R.G.J. Miller, John Wiley & Sons, (1987)
59. M. Moskovits and G.A Ozin, Crypchemistry, Chap 2,Ed. M. Moskovts and G.A. Ozin, Wiley Interscience Publication, New York (1976)
60. R.D. Hunt, L. Andrews, *J. Phys. Chem.* 1992, 96, 6945
61. L. George, K. Sankaran, K.S Viswanathan, C.K. Mathews, *Spectrochim. Acta.* 1995, 51A, 587
62. Gray, Theodore (2009). The Elements: A Visual Exploration of Every Known Atom in the Universe. New York: Black Dog & Leventhal Publishers.
63. T. Steiner, E. B. Starikov, A. M. Amado and J. J. C. Teixeira-Dias, *J. Chem. Soc.* 1995, Perkin Trans. 2, 1321.
64. George, L; Garcia, E; Sander, W*; J. Phys. Chem. A* 2003,107, 6850-6858
65. Matter H^1, Nazaré M, Güssregen S, Will DW, Schreuder H, Bauer A, Urmann M, Ritter K, Wagner M, Wehner V, *Angew Chem*. 2009, 16, 48.
66. A. Endahl, B. Nelander, *Chem. Phys. Lett* 1983, 100, 129
67. R. F. W. Bader, Atoms in Molecules. A Quantum Theory, Clarendon Press, Oxford, 1994
68. *http://www.chemistry.mcmaster.ca/aim/aim_0.html*
69. Yanmei Lan, "Study of Hydrogen Bonding Properties with ab-inito calculations, Neutron Scattering Spectroscopy and 1H NMR", 2007

70. Gautam R. Desiraju, Thomas Steiner, “The weak Hydrogen Bond: In structural Chemistry and Biology” (IUCr) Monographs in Crystallography, Vol. 9. Oxford: Oxford University Press,1999